

ViCA: Efficient Multimodal LLMs with Vision-Only Cross-Attention

Wenjie Liu ^{*1} Hao Wu ^{*1} Xin Qiu ¹ Yingqi Fan ¹
 Yihan Zhang ¹ Anhao Zhao ¹ Yunpu Ma ² Xiaoyu Shen ¹

Abstract

Modern multimodal large language models (MLLMs) adopt a unified self-attention design that processes visual and textual tokens at every Transformer layer, incurring substantial computational overhead. In this work, we revisit the necessity of such dense visual processing and show that projected visual embeddings are already well-aligned with the language space, while effective vision–language interaction occurs in only a small subset of layers. Based on these insights, we propose **ViCA** (Vision-only Cross-Attention), a minimal MLLM architecture in which visual tokens bypass all self-attention and feed-forward layers, interacting with text solely through sparse cross-attention at selected layers. Extensive evaluations across three MLLM backbones, nine multimodal benchmarks, and 26 pruning-based baselines show that ViCA preserves **98%** of baseline accuracy while reducing visual-side computation to **4%**, consistently achieving superior performance–efficiency trade-offs. Moreover, ViCA provides a regular, hardware-friendly inference pipeline that yields **>3.5 \times** speedup in single-batch inference and **>10 \times** speedup in multi-batch inference, reducing visual grounding to *near-zero* overhead compared with text-only LLMs. It is also orthogonal to token pruning methods and can be seamlessly combined for further efficiency gains. Our code is available at <https://github.com/EIT-NLP/ViCA>.

1. Introduction

Large Language Models (LLMs) have demonstrated impressive capabilities across diverse natural language tasks (Brown et al., 2020; OpenAI, 2022; Su et al., 2022;

^{*}Equal contribution ¹Ningbo Key Laboratory of Spatial Intelligence and Digital Derivative, Institute of Digital Twin, Eastern Institute of Technology, Ningbo ²LMU Munich. Correspondence to: Xiaoyu Shen <xyshen@eitech.edu.cn>.

Achiam et al., 2023; Touvron et al., 2023; Su et al., 2024). Building on this success, Multimodal Large Language Models (MLLMs) extend linguistic reasoning to visual contexts, enabling grounded understanding and multimodal interaction (OpenAI, 2023; Li et al., 2023a; Dai et al., 2023; Lin et al., 2024b). Early MLLMs, such as Flamingo (Alayrac et al., 2022) and Blip (Li et al., 2022), adopt a *cross-attention-based* design: visual representations are produced by a visual encoder and injected into the language model exclusively through cross-attention. In contrast, most modern MLLMs have converged to a unified *self-attention-based* design, as exemplified by LLaVA (Liu et al., 2023b;a; 2024b), InternVL (OpenGVLab, 2024; Wang et al., 2025) and QwenVL (Wang et al., 2024; Bai et al., 2025). Under this design, visual features are projected into the textual embedding space and concatenated with text tokens, forming a single token sequence that is processed uniformly by the Transformer (Li et al., 2024b; Lin et al., 2024a). While conceptually simple and highly extensible, it is computationally inefficient: visual tokens are repeatedly updated by self-attention and feed-forward networks (FFNs) at every layer, resulting in substantial overhead (Yang et al., 2025a).

To mitigate this cost, recent work has largely focused on pruning-based acceleration, which dynamically remove visually less important tokens or computational units during inference (Zhang et al., 2025e; Shang et al., 2025; Chen et al., 2024a; Lin et al., 2025). However, such approaches retain the self-attention-based architecture and suffer from two fundamental limitations. First, they rely on elaborate importance estimation mechanisms that prove highly sensitive to input visual redundancy, positional effects, and cross-layer attention variability, making pruning decisions unstable and error-prone (Kim et al., 2025; Wen et al., 2025b). Second, pruning incurs extra system overhead (e.g., full attention map computation, per-layer decisions, dynamic selection and reordering), which leads to highly nonlinear latency behavior and causes practical speedups to fall far short of theoretical FLOPs reductions (Wen et al., 2025a).²

²These overheads are dominated by non-arithmetic GPU costs (e.g., kernel launches, gather/scatter operations, buffering and synchronization) (Fernandez et al., 2023). Even small token-count changes can disrupt kernel grids, FlashAttention tiling and bandwidth, often worsened by GPU tail effect (Eliopoulos et al., 2025).

Prior studies have suggested substantial redundancy in visual computation: Visual attention is largely local (Zhang et al., 2024; Li et al., 2025a). Only a small fraction of FFN channels significantly affects performance (Yuan et al., 2025; Fan et al., 2025), and even in training-free settings, freezing visual updates in certain layers incurs minimal accuracy loss (Yuan et al., 2025). These observations motivate us towards a more fundamental question: *do we truly need to apply sophisticated pruning techniques based on the unified self-attention-based architecture, or is the architecture itself over-engineered for multimodal fusion?*

In this work, we empirically test this hypothesis by freezing visual tokens immediately after projection, completely removing their self-attention and FFN updates. Surprisingly, this aggressive simplification results in only a marginal performance drop, indicating that *projected visual embeddings are already well aligned with the LLM’s semantic space*. In effect, repeated self-attention-based refinement of visual tokens provides little additional benefit. We further investigate where vision–language interaction truly takes place within the Transformer. By analyzing the cosine similarity of text representations before and after text-vision cross-attention at each layer, we observe that effective multimodal interaction is concentrated in only a small subset of layers.

Based on these findings, we propose **ViCA** (Vision-only Cross-Attention): a minimal and efficient MLLM architecture that is conceptually closer to early cross-attention-based models, yet grounded in modern LLM backbones and empirical analysis. In ViCA, visual tokens bypass self-attention and FFNs entirely, and vision–language interaction is realized solely through sparse cross-attention at a small set of key layers. We validate ViCA through extensive experiments across three representative MLLM backbones and nine widely used multimodal benchmarks covering diverse vision–language reasoning tasks. The results show that ViCA preserves 98% of baseline accuracy, while reducing visual-side computation to 4% of the original architecture. To ensure a rigorous and fair comparison, we benchmark our approach against 26 existing pruning methods, encompassing both token-level and operation-level strategies. Across all tested settings, ViCA consistently achieves superior performance–efficiency trade-offs, demonstrating that *architecturally eliminating redundant visual computation is more effective than dynamically pruning it within a self-attention-based framework*.

Importantly, ViCA introduces an asymmetric attention structure: queries originate exclusively from text tokens, while keys and values come from both text and visual tokens. This aligns naturally with FlashAttention, which natively supports short-query–long-key/value attention by setting the causal mask to the bottom-right corner of the attention matrix (Dao, 2024). As a result, FlashAttention kernels can

be applied efficiently without the need to construct full attention maps or trigger kernel behavior degradation as in pruning-based methods. In practice, this reduces end-to-end latency to a level *close to that of the original text-only Transformer*, meaning that incorporating visual information incurs *near-zero* additional runtime overhead, a regime that prior MLLM acceleration methods have not achieved. Finally, ViCA is orthogonal to existing token-dropping techniques and can be combined with them for further efficiency gains. For example, by directly integrating PDrop (Xing et al., 2024b) in a training-free manner, we further reduce visual computation to 2% of the original architecture with over 96% performance maintenance. In summary, our main contributions are as follows:

(1) **Architectural necessity analysis.** We show that visual token updates via self-attention and FFN are largely unnecessary in self-attention LVLMs, and that effective cross-modal interaction is confined to a small subset of layers.

(2) **Minimal and efficient architecture.** Based on these insights, we propose ViCA (Vision-only Cross-Attention), which eliminates redundant computation and enables a fully regular, hardware-friendly inference pipeline.

(3) **Extensive empirical validation.** We evaluate ViCA across three MLLM backbones and nine widely used multimodal benchmark, and compare it with 26 existing pruning methods. ViCA consistently performs the best, preserving 98% of baseline accuracy while reducing visual-side computation to 4%. It achieves $> 3.5 \times$ speedup in single-batch inference and $> 10 \times$ speedup in multi-batch inference, reducing multimodal latency close to text-only models.

2. Related Work

The quadratic cost of attention with respect to sequence length motivates token pruning in MLLMs, which reduces the effective number of visual tokens processed by the LLM. A prevalent line of work ranks visual tokens by importance and removes low-saliency ones. FastV (Chen et al., 2024b), PyramidDrop (Xing et al., 2024a), and SparseVLM (Zhang et al., 2025e) estimate token importance via text-to-vision cross-attention. FiTPruner (Ye et al., 2025a), FiCoCo-L (Han et al., 2024), ATP-LLaVA (Ye et al., 2025b), and HiMAP (Yin et al., 2025) further incorporate vision-to-vision cues to capture intra-visual redundancy. Model-guided signals are explored in SGL (Zhao et al., 2025b), Dynamic-LLaVA (Huang et al., 2024), LVPruning (Sun et al., 2025), and TwigVLM (Shao et al., 2025). To mitigate information loss under aggressive pruning, PACT (Dhouib et al., 2025), TokenCarve (Tan et al., 2025), and SparseVLM (Zhang et al., 2025e) apply cyclic merging that aggregates discarded tokens into compact representatives.

While token pruning reduces computation by shortening

the visual token sequence, it leaves the underlying self-attention-based architecture. Operation pruning going further to reduce operator- and submodule-level redundancy by skipping or sparsifying internal computations (Zhao et al., 2025a; Han et al., 2025; Qiu et al., 2025; Ding et al., 2026). For example, ShortV (Yuan et al., 2025) provides layer-wise evidence by freezing visual-token updates one layer at a time and revealing substantial depth-wise redundancy. At the module level, Skip-Vision (Zeng et al., 2025) focuses on the FFN by skipping the FFN sublayer for visual tokens in selected layers, whereas YOPO (Zhang et al., 2024) and RedundancyLens (Li et al., 2025a) focus on attention sparsification by restricting vision-to-vision attention to local windows, and additionally prune a subset of FFN dimensions. Along this direction, DOP (Liu et al., 2025a) skips both attention and FFN operations on visual tokens. While existing methods often use redundancy analyses to motivate pruning heuristics, our work turns attention and FFN redundancy diagnostics into an explicit minimal necessary architecture and verifies its necessity through experiments.

3. Information-Flow View: Self-Attention vs. Cross-Attention Interaction

Building on prior efficient MLLM studies (Zhang et al., 2025f; Yin et al., 2025; Yang et al., 2025b; Li et al., 2025a; Tong et al., 2025), we present an information-flow view to precisely define what is being pruned. We distinguish **self-attention** and **cross-attention** interaction patterns by how visual tokens participate in attention and FFN computation. Let $H^{(l)} = [V^{(l)}; T^{(l)}]$ be the concatenation of visual and text tokens at layer l . A self-attention layer can be written in a blockwise form as follows:

$$\begin{aligned}\tilde{H}^{(l)} &= \begin{bmatrix} \tilde{V}^{(l)} \\ \tilde{T}^{(l)} \end{bmatrix} = H^{(l)} + \begin{bmatrix} A_{VV} & A_{VT} \\ A_{TV} & A_{TT} \end{bmatrix} \begin{bmatrix} V^{(l)} \\ T^{(l)} \end{bmatrix} W_V \\ H^{(l+1)} &= \tilde{H}^{(l)} + \begin{bmatrix} \text{FFN}_V(\tilde{V}^{(l)}) \\ \text{FFN}_T(\tilde{T}^{(l)}) \end{bmatrix}\end{aligned}$$

where $A = \text{softmax}(QK^\top/\sqrt{d})$ is induced by masked self-attention over the unified sequence (we omit multi-head/output projections for brevity). All tokens share the same value projection W_V , following standard self-attention; the block form only reflects token-level information flow. In the common decoder-only setting with a causal mask and vision tokens placed as a prefix, the mask enforces $A_{VT} = 0$, leaving three active channels: V2V (A_{VV}), T2V (A_{TV}), and T2T (A_{TT}). As illustrated in Fig. 1, **self-attention** performs joint *read-write* over $[V; T]$: visual tokens are *updated* via V2V attention and the visual FFN branch $\text{FFN}_V(\cdot)$, while text tokens *read* vision through A_{TV} and interact within text via A_{TT} and $\text{FFN}_T(\cdot)$.

In contrast, **cross-attention** treats visual tokens as *read-only* memory: text queries attend to visual keys/values, while vi-

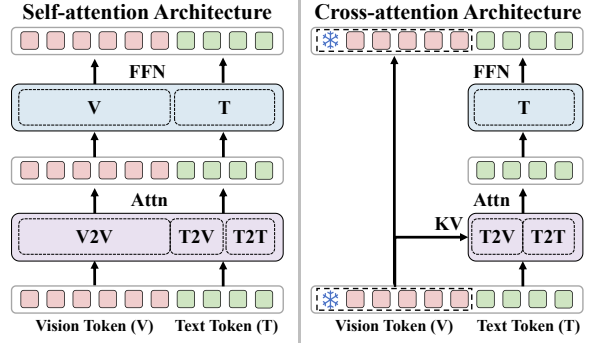


Figure 1. Comparison between self-attention and cross-attention architectures from an information-flow perspective. Attention and FFN operations for visual tokens dominate the computation in MLLM. The V2V, T2V, and T2T denote vision-to-vision, text-to-vision, and text-to-text attention, respectively.

sual tokens are *frozen* and not updated by either attention or FFN, i.e., enforcing $\Delta V^{(l)} = 0$ by bypassing all visual write operations. This “freeze-vision” intuition is supported by prior evidence that *visual-token writes have heavy redundancy* (Yuan et al., 2025). Different from such training-free analyses, our approach is training-based and leverages this redundancy to redesign interaction paths.³ This read-only design for visual tokens is conceptually related to early cross-attention-based MLLMs, such as Flamingo (Alayrac et al., 2022) and Blip (Li et al., 2022), where vision features are computed once and exposed to the language model through cross-attention as KV memory. While such early MLLMs avoid repeated visual updates, they typically rely on modality-specific cross-attention or two-stream architectures, which limit deep fusion and require careful architectural customization. Consequently, recent MLLMs have largely converged to self-attention-based designs that unify vision and language tokens into a single sequence, enabling stronger cross-modal interaction with greater architectural simplicity. Our analysis revisits this trade-off and motivates architectures that retain unified modeling while avoiding redundant visual-token writes.

4. Methodology

4.1. Motivation: Where Visual Information Matters

Building on the information-flow view introduced in Section 3, we empirically examine how visual-token *writes* and cross-modal *reads* influence the final model output.

Impact Measurement of Visual Updates. To operationalize the information-flow perspective, we use two comple-

³In Appendix C.3 and Tab. 12, we further illustrate the details of FLOPs calculation, showing that visual-write operations dominate vision-side FLOPs (often over 80%), highlighting the efficiency advantage of such read-only architecture.

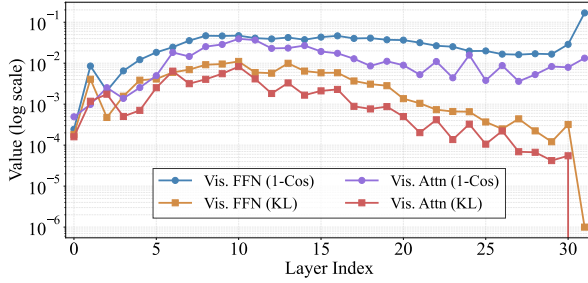


Figure 2. Layer-wise diagnostics of visual-token updates in LLaVA-1.5-7B on TextVQA, showing output impact (Vis Attn/FFN KL) and representation change (Vis Attn/FFN 1-Cos).

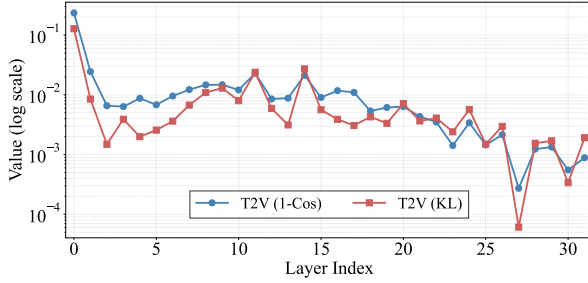


Figure 3. Layer-wise diagnostics of text-to-vision (T2V) cross-attention in LLaVA-1.5-7B on TextVQA, showing output impact (T2V KL) and representation change (T2V 1-Cos).

mentary metrics to capture representation change and output impact. Representation change is measured by the cosine similarity between token embeddings before and after a given module:

$$\text{Cos}(h, h') = \frac{h^\top h'}{\|h\| \|h'\|},$$

where h and h' denote token embeddings before and after the update. Output impact is measured by the KL divergence between the original output distribution $p(y)$ and the distribution obtained after disabling the update:

$$\text{KL}(p \parallel p') = \sum_y p(y) \log \frac{p(y)}{p'(y)}.$$

Intuitively, cosine similarity quantifies how much representations are modified, while KL divergence indicates whether such modifications propagate to the final output distribution.

Redundancy in Vision-Token Write. We rank Transformer layers by the two impact metrics defined above. As shown in Fig. 2, cosine similarity indicates substantial representation changes across a broad range of early-to-mid layers (layers 6–17 for attention and 5–31 for FFN). In contrast, KL-based diagnostics reveal that only a much narrower subset (layers 6–11 for attention and 5–11 for FFN) meaningfully affects the final output. Beyond these layers, visual representations continue to change, but their contribution to model

Table 1. Redundancy diagnosis in LLaVA-1.5-7B (TF: training-free; T: training-based). Removing all vision-update attention/FFN (frozen in table), and keeping T2V Attention only in essential layers yield negligible performance change after training. Details in Appendix Table 8.

Setup	Retained Layers	Layer Indices	MME ^P	GQA	VQA ^T	POPE	Avg. (%)
Baseline							
-	Full	0–31	1506.5	61.9	58.2	86.8	100.0
Vision-Update Attention							
TF	Essential	6–11	1454.5	61.0	56.1	86.7	98.3
	Over-approx.	6–17	1469.7	61.6	56.6	86.0	98.8
	Non-essential	0–5,12–31	1361.2	59.2	55.4	83.9	95.3
	Frozen	-	1298.2	54.5	51.0	79.8	91.7
T	Frozen	-	1501.1	62.1	57.1	87.1	100.2
Visual-Update FFN							
TF	Essential	5–11	1463.2	58.9	54.2	85.2	96.8
	Non-essential	0–4,12–31	988.6	49.8	48.9	65.4	81.8
	Frozen	-	876.8	39.6	40.9	61.1	71.2
T	Essential	5–11	1475.7	63.3	58.2	87.3	100.5
	Frozen	-	1472.4	62.0	56.9	87.3	99.2
Text-to-Vision Cross-Attention							
TF	Essential	0–1,7–11,14	1393.5	54.4	51.3	86.1	93.5
	Non-essential	2–6,12–13,15–31	758.1	44.8	45.4	70.4	63.0
	Frozen	-	572.1	29.9	29.9	50.3	46.2
T	Essential	0–1,7–11,14	1476.6	62.7	56.4	87.1	99.5

predictions becomes negligible. Guided by this ranking, we group layers into three regimes: *full* (all visual updates retained), *essential* (updates kept only in top-ranked layers), and *none* (all visual-token updates removed). We evaluate these settings under both training-free (TF) and training-based (T) protocols, with results summarized in Table 1. In the training-free setting, retaining only the essential layers largely preserves performance across benchmarks. Under training-based adaptation, performance is almost fully recovered even when all visual-token updates are frozen. These results indicate that *a large fraction of visual-token updates, especially in deeper layers, is functionally redundant, and that any loss incurred by removing them can be rapidly compensated through fine-tuning.*

Redundancy in Cross-Modal Read. Prior studies suggest that visual information is incorporated into language representations primarily through text–vision (T2V) cross-attention (Zhang et al., 2025g). Consistent with this view, Fig. 3 shows that effective cross-modal information injection is concentrated in a small number of early and mid layers, with a prominent peak around layer 10 in LLaVA-1.5-7B. Beyond these layers, visual-token updates rarely propagate back to text representations, explaining why later updates, despite modifying representations, have little impact on the final output. Table 1 further confirms that restricting text–vision cross-attention and visual updates to these essential layers largely preserves performance. These observations suggest that *once cross-modal information is injected through a small set of cross-attention layers, subsequent visual-token updates become largely redundant.*

4.2. ViCA: Vision-Only Cross-Attention

Motivated by the above diagnostics, we introduce **ViCA**, a minimal architectural modification. Fig. 4 contrasts ViCA with token-dropping approaches and illustrates its design:

(1) Removing visual token write operations: Visual tokens no longer participate in self-attention or feed-forward updates at any transformer layer. After the initial projection, visual token representations remain fixed and are not written by either attention or FFN modules. Importantly, this differs from freezing the vision encoder: ViCA operates entirely within the language model and does not prevent the vision encoder itself from being fine-tuned.

(2) Sparse cross-modal read operations: To preserve effective vision-to-language read path, text-to-vision cross-attention is retained only at a small set of diagnostically identified key layers. In these layers, visual tokens serve as static keys and values that text tokens can attend to, while all remaining layers operate purely on text tokens.

Together, these designs yield a streamlined computation graph in which *visual-token writes are entirely removed and cross-modal read is confined to a few critical layers*. This restructuring eliminates the dominant sources of redundant visual computation during pre-filling, substantially reducing vision-side cost while preserving the cross-modal information flow necessary for downstream performance.

4.3. Practical Acceleration and System Compatibility

Comparison with Token Pruning. Most token-pruning methods estimate acceleration using token counts or FLOPs, yet these metrics fail to capture dominant GPU overheads, including kernel launches, data movement, and synchronization (Fernandez et al., 2023), as well as the runtime cost of pruning itself, such as importance scoring and token selection (Wen et al., 2025a). Moreover, dynamically changing token counts induce frequent reconfiguration of attention kernels and FlashAttention tiling, leading to highly nonlinear latency behavior that often decouples practical speedup from theoretical FLOPs reduction (Eliopoulos et al., 2025; NVIDIA, 2023). In contrast, ViCA targets the computation *architecture* rather than the sequence length. By keeping token counts and attention shapes fixed across layers while removing visual-token write paths (i.e., excluding visual tokens from attention queries and FFNs), ViCA avoids dynamic shapes, kernel reconfiguration, and unnecessary data movement. As a result, the reduced computation maps more directly and reliably to real-world inference speedups.

Compatibility with FlashAttention. In ViCA, some layers perform text-only attention. In other layers, queries come from text tokens, and KVs include both text and visual tokens. Since FlashAttention v2.1+ supports this ($q_{len} < kv_{len}$) pattern under causal masking by aligning

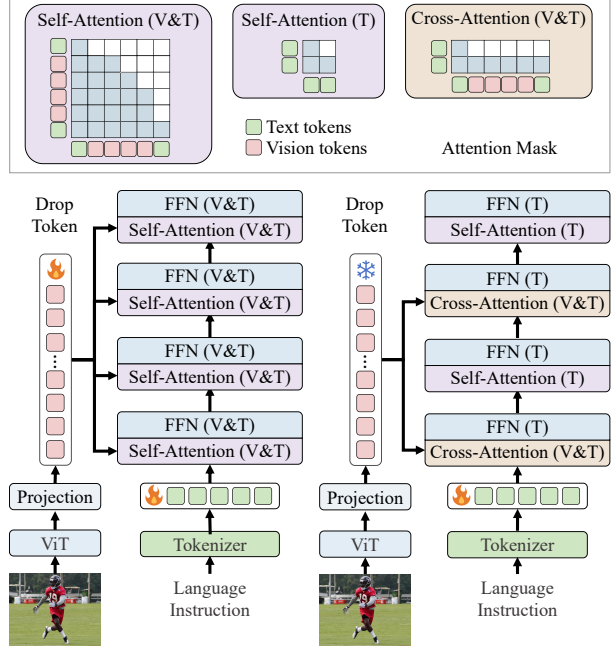


Figure 4. Common token dropping vs. our minimal architecture (ViCA). Left: Token dropping removes some visual tokens, but the remaining ones still undergo full self-attention and FFN updates across layers, incurring substantial visual computation. Right: ViCA removes visual update paths in attention and FFN. Visual tokens act only as KVs in a few cross-attention layers, while all other operations run on text tokens, reducing visual computation.

the mask to the bottom-right corner. By simplifying the vision computation graph without modifying token sequence lengths or attention tensor shapes, ViCA preserves full compatibility with efficient attention kernels and existing inference optimizations. (see Appendix C.4 for details).

Orthogonality to Token Pruning. ViCA prunes redundant visual computation paths instead of tokens, making it orthogonal to existing token-dropping approaches. These methods can be combined at inference time to further reduce visual computation with minimal performance impact. Unlike most token pruning methods, which assume visual importance decreases with depth (Xing et al., 2024b), ViCA restricts visual tokens to cross-attention in fewer layers, avoiding unnecessary retention of tokens in layers where they provide little benefit. This makes ViCA a more effective and interpretable foundation for token pruning.

5. Experiments

5.1. Setup

Models. Within the LLaVA-1.5 architecture (Liu et al., 2024a), we evaluate our approach using three different LLM backbones: MobileLLaMA-2.7B (Wu et al., 2024), Vicuna-7B-v1.5 (Zheng et al., 2023), and Vicuna-13B-v1.5 (Zheng et al., 2023). In this paper, we denote the resulting models

Table 2. Performance comparison of different pruning approaches on LLaVA-1.5-7B across nine benchmarks. The table reports per-benchmark accuracy and the average performance relative to the original model. Methods are grouped by pruning strategy: no background color indicates training-free methods, red denotes training-based pruning, and blue highlights our approach. ViCA refers to the model retrained under the proposed minimal efficient architecture using the standard two-stage pretraining and fine-tuning pipeline. ViCA+PDrop[†] further applies PyramidDrop at inference time. Op and Tok denote operation-level and token-level pruning methods, respectively. Vision-related computation and token counts are measured following the FLOPs formulation in Appendix C.3.

Method	Sparsity Op. Tok.	Vision-side Token TFLOPs (Rel.)		MME ^P	MMB	MMB ^{CN}	GQA	VQA ^{V2}	SQA ^I	VQA ^T	POPE	SEED ^I	Rel. Avg.
		Token	TFLOPs (Rel.)										
LLaVA-1.5-7B	- -	576	7.65 (100.0%)	1506.5	64.7	58.1	61.9	78.5	69.5	58.2	86.8	66.2	100.0%
ToMe	✓	64	0.83 (10.9%)	-	43.7	38.9	48.6	57.1	50.0	45.3	52.5	-	70.9%
PDrop	✓	64	0.83 (10.9%)	1309.2	58.8	50.5	47.5	69.2	69.0	50.6	55.9	-	85.0%
HiRED	✓	64	0.83 (10.9%)	-	60.2	51.3	54.6	69.7	68.2	44.2	73.6	-	88.2%
HiPrune	✓	64	0.83 (10.9%)	-	59.5	53.4	53.6	69.2	68.9	54.9	73.0	-	90.9%
FlowCut	✓	64	0.83 (10.9%)	-	60.8	55.4	55.6	72.8	69.1	55.6	80.2	-	94.2%
HoloV	✓	64	0.83 (10.9%)	-	63.3	55.1	55.3	72.8	69.5	55.4	80.3	-	94.6%
VISA	✓	64	0.83 (10.9%)	1420.6	62.1	57.3	56.2	67.9	55.6	77.6	-	-	94.6%
D ² Pruner	✓	64	0.83 (10.9%)	-	61.9	55.6	57.9	74.6	70.0	56.1	82.4	-	96.0%
VScan	✓	64	0.83 (10.9%)	-	62.1	55.7	58.3	75.4	69.1	55.6	85.0	-	96.4%
FiCoCo-L	✓	58	0.75 (9.9%)	-	61.5	53.3	53.2	69.7	69.5	55.7	82.1	-	93.1%
FastV	✓	32	0.42 (5.4%)	884.6	37.8	33.2	41.5	43.4	42.6	42.5	32.5	-	58.6%
SparseVLM	✓	32	0.42 (5.4%)	1046.7	51.4	40.6	48.3	58.6	57.3	46.1	67.9	-	76.4%
VisPruner	✓	32	0.42 (5.4%)	1271.0	58.4	52.7	52.2	67.7	69.2	53.9	72.7	54.3	88.2%
DivPrune	✓	32	0.42 (5.4%)	1284.9	57.6	49.1	54.9	71.2	68.6	52.9	81.5	58.7	90.0%
DOP _V	✓	32	0.42 (5.4%)	1306.5	59.4	53.7	54.8	71.0	69.1	54.5	79.6	56.7	91.2%
CDPruner	✓	32	0.42 (5.4%)	1373.0	59.6	49.6	57.0	73.6	69.5	53.2	87.9	-	93.2%
DOP _{CD}	✓	32	0.42 (5.4%)	1397.5	60.1	52.2	58.1	74.7	69.3	54.2	87.9	82.2	94.7%
PDrop	✓	270	3.54 (46.3%)	1490.1	63.9	56.7	61.7	78.7	70.1	57.7	86.9	65.8	99.4%
Dynamic-LLaVA	✓	115	1.50 (19.6%)	1479.8	65.4	-	61.4	78.0	69.1	57.0	85.0	64.6	98.8%
YOPO	✓	70	0.92 (12.0%)	1423.5	64.6	57.0	60.7	77.4	68.0	55.2	86.6	64.6	97.7%
TwigVLM	✓	64	0.83 (10.9%)	1404.0	60.4	53.8	61.2	75.6	70.0	55.8	82.7	56.9	94.7%
VisionZip	✓	64	0.83 (10.9%)	-	61.5	-	57.0	74.2	68.8	56.0	80.9	-	95.0%
DART	✓	64	0.83 (10.9%)	-	64.7	56.7	57.1	74.6	71.1	54.7	79.3	-	96.1%
LLaVA-PruMerge	✓	32	0.42 (5.4%)	1350.3	60.9	50.0	57.2	72.0	68.5	56.0	76.3	50.7	90.4%
TRIM	✓	29	0.38 (4.9%)	1415.4	63.3	46.6	58.4	71.5	67.9	49.1	84.8	61.8	92.3%
TokenPacker	✓	16	0.21 (2.7%)	1378.8	62.7	-	58.9	74.4	68.1	52.5	83.7	-	94.7%
Delta-LLaVA	✓	16	0.21 (2.7%)	1375.9	62.9	-	59.5	73.1	69.7	53.6	84.7	-	95.4%
ViCA (ours)	✓	24	0.31 (4.1%)	1464.5	64.0	57.7	60.4	76.6	68.5	55.5	86.7	63.2	97.8%
ViCA+PDrop [†] (ours)	✓	12	0.16 (2.0%)	1449.7	63.3	56.9	59.0	75.8	69.3	54.4	85.2	60.8	96.3%

as LLaVA-1.5-3B, LLaVA-1.5-7B, and LLaVA-1.5-13B, respectively. Details are provided in Appendix C.1.

Benchmarks. We conduct experiments on nine widely adopted image-based benchmarks, including MME^P (Fu et al., 2023), MMB (Liu et al., 2025c), MMB^{CN} (Liu et al., 2025c), GQA (Hudson & Manning, 2019), VQA^{V2} (Goyal et al., 2017), ScienceQA-Image (SQA^I) (Lu et al., 2022), TextVQA (VQA^T) (Singh et al., 2019), POPE (Li et al., 2023b), and SEED-Image (SEED^I) (Li et al., 2024a). Details are provided in Appendix E.

Implement Details. We adopt LLaVA-1.5 as our experimental platform because it is a widely used open-source MLLM and a representative testbed for multimodal token compression. Its fully public training data and pipeline, together with a well-established two-stage recipe, enable reproducible and apples-to-apples comparisons. In the training-based setting, we follow the official data and two-stage protocol (Liu et al., 2024a), train from scratch with reduced visual computation, and keep the total iterations identical to the original model. All experiments are conducted on A100 GPUs.

Efficiency Evaluation. To evaluate practical efficiency, inference is benchmarked on 5,000 TextVQA samples using

an NVIDIA A6000 GPU. Specifically, the A6000 GPU’s moderate compute capability keeps both the baseline and the proposed method close to saturated CUDA utilization, so observed speedups primarily reflect computation reduction rather than hardware underutilization. Accordingly, we report CUDA utilization and prefill-stage latency, since prefill dominates overall inference cost.

5.2. Main Results

Task Performance. We evaluate ViCA and its inference-time combination with PDrop on nine benchmarks across the LLaVA-1.5 family. All token counts are reported as equivalent visual tokens based on vision-side FLOPs (see Appendix C.3 for details). On LLaVA-1.5-7B (Table 2), ViCA preserves 97.8% of full-model accuracy while using only 4.1% of vision computation (24 tokens). When combined with PyramidDrop, ViCA+PDrop further reduces computation to 2.0% (12 tokens) and still achieves 96.3% accuracy, outperforming existing training-free and training-based methods under comparable or even larger budgets. This trend is consistent across model scales (Appendix Table 7): on LLaVA-1.5-3B, ViCA recovers 98.7% accuracy at 4.5% computation (27 tokens), while ViCA+PDrop main-

Table 3. Theoretical efficiency comparison across three LLM backbones within the LLaVA-1.5 framework.

Base Model	Method	Vision Tokens	Vision TFLOPs	Total TFLOPs	Vision KV-Cache	Rel. Avg.
LLaVA-1.5-3B	Original PDrop	576	3.04	3.33	100.0%	100.0%
	ViCA	27	0.14↓95.5%	0.42	28.1%	98.7%
	ViCA+PDrop [†]	12	0.06↓98.0%	0.34	12.5%	98.2%
LLaVA-1.5-7B	Original PDrop	576	7.65	8.38	100.0%	100.0%
	ViCA	24	0.31↓95.9%	1.02	25.0%	97.8%
	ViCA+PDrop [†]	12	0.16↓98.0%	0.87	12.5%	96.3%
LLaVA-1.5-13B	Original PDrop [†]	576	14.91	16.34	100.0%	100.0%
	ViCA	19	0.49↓96.7%	1.88	20.0%	97.0%
	ViCA+PDrop [†]	10	0.26↓98.3%	1.66	10.6%	96.3%

Table 4. Practical efficiency comparison of three LLM backbones in the LLaVA-1.5 framework under FlashAttention. We report the baseline efficiency, text-only efficiency, and the efficiency achieved by our method. All results are averaged over 5,000 TextVQA samples on an NVIDIA A6000 GPU.

Base Model	Method	CUDA Util	Latency. (SpdUp)	Latency Vis. (Rel.)
LLaVA-1.5-3B	Original	78%	57.9 (1.0×)	35.6 (100.0%)
	w/o Vis. Tok.	70%	22.3 (2.6×)	0.0 (0.0%)
	Ours	65%	24.2 (2.4×)	1.9 (5.3%)
LLaVA-1.5-7B	Original	97%	124.5 (1.0×)	94.2 (100.0%)
	w/o Vis. Tok.	95%	30.3 (4.1×)	0.0 (0.0%)
	Ours	94%	36.0 (3.5×)	5.7 (6.1%)
LLaVA-1.5-13B	Original	97%	210.6(1.0×)	159.3 (100.0%)
	w/o Vis. Tok.	90%	51.3(4.1×)	0.0 (0.0%)
	Ours	98%	59.3(3.6×)	8.0 (5.0%)

tains 98.2% accuracy at 2.0% computation (12 tokens); on LLaVA-1.5-13B, ViCA achieves 97.0% accuracy with only 3.3% computation (19 tokens). Overall, ViCA consistently attains higher accuracy under substantially reduced visual computation budgets.

Complementarity with Token Pruning. Our approach removes redundant visual-token update paths at the architectural level, making it inherently orthogonal to token-dropping methods that operate on token selection. As a result, ViCA can be seamlessly combined with PyramidDrop at inference time without modifying the training procedure. This combination further reduces vision-related computation to 1.7%–2.0% across LLaVA-1.5-3B, 7B, and 13B models, while incurring only a modest 1.8%–3.7% accuracy drop relative to the original full models. These results confirm that architectural-level visual compute removal and token-level pruning are complementary. Implementation details of PyramidDrop are provided in Appendix C.2.

Theoretical Efficiency. As shown in Table 3, under the proposed minimal and efficient architecture, the vision-related computation of LLaVA-1.5-3B/7B/13B is reduced to 4.5%/4.1%/3.3% of the original models. Under the FLOPs-based analysis, this reduction is equivalent to compress-

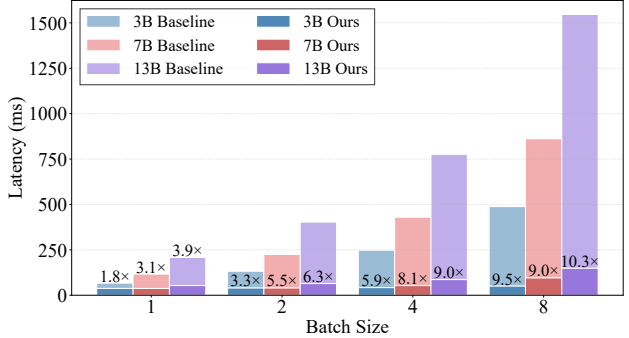


Figure 5. Latency and speedup of forward pass on A6000 GPU with increasing batch sizes. Pre-training forward-pass latency of our model variants compared to the original baseline model (averaged over 100 samples). Speedup ratios are annotated on the stacked bars for LLaVA-1.5-3B, 7B, and 13B.

ing the number of visual tokens from 576 to 27/24/19, respectively. Correspondingly, the visual KV-cache sizes are reduced to 28.1%/25.0%/20.0% of the original. When combined with PyramidDrop at inference time, the vision-related computation is further reduced to 2.0%/2.0%/1.7%, corresponding to 12/12/10 equivalent visual tokens, with the visual KV-cache sizes reduced to 12.5%/12.5%/10.6% of the original.

Practical Efficiency. In multimodal inference, the prefill stage dominates computation and end-to-end latency because it processes all visual tokens and incurs most vision-related overhead. We therefore focus our analysis on prefill performance. As shown in Table 4, ViCA achieves prefill latency close to that of the text-only model, yielding speedups of 2.4× / 3.5× / 3.6× over the original LLaVA-1.5 3B / 7B / 13B models. Figure 5 further shows that these gains persist across batch sizes, with stable speedup trends and larger absolute latency reductions for larger models. The smaller speedup on the 3B model mainly results from reduced CUDA utilization. As visual computation is aggressively removed, fewer streaming multiprocessors (SMs) are scheduled, leaving some previously active SMs underutilized. In contrast, the 7B and 13B models operate near saturation and translate computation reduction more effectively into latency gains. Finally, isolating the latency introduced by visual computation by subtracting the text-only prefill latency shows that ViCA accounts for only 5.0%–6.1% of the original visual latency. This closely matches the theoretical visual computation ratios of 3.3%–4.5% in Table 4, validating our FLOPs-based analysis. We measure the prefill forward-pass latency across batch sizes to simulate multi-batch inference. As shown in Figure 5, at batch size 8, ViCA achieves approximately 10× speedup over the original LLaVA-1.5 models.

Parallel Decoupling. Under ViCA, vision-side computation is confined to two components: linear projections

Table 5. Performance comparison on LLaVA-1.5-7B under different visual token update freezing strategies. Results across nine benchmarks are reported for three freezing variants, evaluated after standard two-stage retraining.

#	Frozen Update		MME ^P	MMB	MMB ^{CN}	GQA	VQA ^{V2}	SQA ^I	VQA ^T	POPE	SEED ^I	Rel. Avg.
	Vis. Attn	Vis. FFN										
1	✗	✗	1506.5	64.7	58.1	61.9	78.5	69.5	58.2	86.8	66.2	100.0%
2	✓	✗	1501.1	66.1	59.5	62.1	78.0	69.3	57.1	87.1	65.8	100.2%
3	✗	✓	1472.4	65.6	56.9	62.0	77.5	70.3	56.9	87.3	64.6	99.2%
4	✓	✓	1471.1	65.2	56.8	61.8	77.2	69.8	56.6	86.8	64.0	98.8%

Table 6. Performance comparison across LLaVA-1.5-3B, 7B, and 13B under different architectural variants. We compare the original dense self-attention model (Original), a dense cross-attention variant with frozen visual-token updates (FreezeVis), and the proposed minimal efficient architecture with sparse cross-attention at selected layers (ViCA). All variants are trained with the standard two-stage protocol and evaluated on nine benchmarks. Computation metrics follow the FLOPs formulation in Appendix C.3.

Base Model	Method	MME ^P	MMB	MMB ^{CN}	GQA	VQA ^{V2}	SQA ^I	VQA ^T	POPE	SEED ^I	Rel. Avg.	Vis. FLOPs
LLaVA-1.5-3B	Original	1258.2	57.0	28.6	59.4	75.3	60.0	48.6	86.4	60.1	100.0%	100.0%
	FreezeVis	1212.0	54.8	34.9	57.5	72.8	61.2	46.8	86.5	57.8	100.3%	16.0%
	ViCA	1188.9	55.4	33.2	56.6	72.1	61.2	45.4	86.2	56.7	98.7%	4.5%
LLaVA-1.5-7B	Original	1506.5	64.7	58.1	61.9	78.5	69.5	58.2	86.8	66.2	100.0%	100.0%
	FreezeVis	1471.1	65.2	56.8	61.8	77.2	69.8	56.6	86.8	64.0	98.8%	16.2%
	ViCA	1464.5	64.0	57.7	60.4	76.6	68.5	55.5	86.7	63.2	97.8%	4.1%
LLaVA-1.5-13B	Original	1529.9	68.5	63.5	63.3	80.0	72.8	61.2	87.0	68.2	100.0%	100.0%
	FreezeVis	1474.5	67.3	60.7	62.4	78.2	71.0	58.2	86.9	66.2	97.4%	16.3%
	ViCA	1453.6	67.1	62.3	61.8	77.9	72.2	56.7	86.5	65.2	97.0%	3.3%

that map visual tokens to key–value representations and the matrix multiplications in text–vision cross-attention. For LLaVA-1.5-7B, the computation ratio between visual key–value projection and cross-attention is approximately 204:1 (Appendix C.3). By freezing visual tokens, ViCA enables parallel decoupling, allowing raw visual tokens to be directly fed into the key–value projection module and precomputed in parallel with the Transformer backbone. As a result, the remaining $\sim 4\%$ vision-side computation can be parallelized, effectively reducing visual latency to near zero.

5.3. Ablation Studies

Freezing Visual Token Updates. We first analyze LLaVA-1.5-7B by independently freezing the attention and FFN update paths of visual tokens. As shown in Table 5, freezing attention updates slightly improves relative average accuracy by 0.2%, whereas freezing FFN updates results in a 0.8% drop, indicating that attention-based visual-token updates are less critical than FFN-based updates. We then freeze both update paths across LLaVA-1.5-3B, 7B, and 13B models. As summarized in Table 6, the resulting models retain 100.3%, 98.8%, and 97.4% of their respective baseline accuracies, while reducing visual computation to approximately 16% of the original, demonstrating that disabling visual-token updates largely preserves performance while substantially reducing visual computation.

Key Cross-attention Layer Selection. As shown in Table 6, disabling visual-token updates while retaining dense

cross-attention (FreezeVis) preserves nearly full accuracy, and further restricting cross-attention to a small set of diagnostically identified key layers (ViCA) incurs only a 1–3% accuracy drop while reducing vision-related FLOPs from approximately 16% to 4%. These results show that visual tokens need not be continuously updated across all Transformer layers and that multimodal reasoning relies on only a small subset of critical text–vision cross-attention layers, supporting the proposed minimal and efficient architecture.

6. Conclusion

In this work, we conduct a systematic architectural diagnosis of self-attention LLMs and find that continuously updating visual tokens via self-attention and FFN layers is largely redundant, while effective cross-modal interaction is concentrated in a small subset of critical layers. Based on this insight, we propose ViCA, which removes redundant visual computation paths and yields a more regular, hardware-friendly inference pipeline, achieving approximately $3.5\times$ prefill speedup in single-batch inference and $> 10\times$ speedup in multi-batch inference. The resulting minimal efficient architecture is also naturally compatible with existing token dropping methods, enabling further efficiency gains when combined. Looking forward, we will explore adaptive architectures for improved cross-modal fusion and aim to unify diverse pruning paradigms into a general framework for efficient and scalable multimodal architectures.

References

Achiam, J., Adler, S., Agarwal, S., Ahmad, L., Akkaya, I., Aleman, F. L., Almeida, D., Altenschmidt, J., Altman, S., Anadkat, S., et al. Gpt-4 technical report. *arXiv preprint arXiv:2303.08774*, 2023.

Alayrac, J.-B., Donahue, J., Luc, P., Miech, A., Barr, I., Hasson, Y., Lenc, K., Mensch, A., Millican, K., Reynolds, M., et al. Flamingo: a visual language model for few-shot learning. *Advances in neural information processing systems*, 35:23716–23736, 2022.

Alvar, S. R., Singh, G., Akbari, M., and Zhang, Y. Divprune: Diversity-based visual token pruning for large multimodal models. In *Proceedings of the Computer Vision and Pattern Recognition Conference*, pp. 9392–9401, 2025.

Arif, K. H. I., Yoon, J., Nikolopoulos, D. S., Vandieren-donck, H., John, D., and Ji, B. Hired: Attention-guided token dropping for efficient inference of high-resolution vision-language models. In *Proceedings of the AAAI Conference on Artificial Intelligence*, pp. 1773–1781, 2025.

Bai, S., Chen, K., Liu, X., Wang, J., Ge, W., Song, S., Dang, K., Wang, P., Wang, S., Tang, J., et al. Qwen2. 5-vl technical report. *arXiv preprint arXiv:2502.13923*, 2025.

Bolya, D., Fu, C.-Y., Dai, X., Zhang, P., Feichtenhofer, C., and Hoffman, J. Token merging: Your ViT but faster. In *International Conference on Learning Representations*, 2023.

Brown, T., Mann, B., Ryder, N., Subbiah, M., Kaplan, J. D., Dhariwal, P., Neelakantan, A., Shyam, P., Sastry, G., Askell, A., et al. Language models are few-shot learners. *Advances in neural information processing systems*, 33: 1877–1901, 2020.

Chen, J., Ye, L., He, J., Wang, Z.-Y., Khashabi, D., and Yuille, A. Efficient large multi-modal models via visual context compression. In *The Thirty-eighth Annual Conference on Neural Information Processing Systems*, 2024a.

Chen, L., Zhao, H., Liu, T., Bai, S., Lin, J., Zhou, C., and Chang, B. An image is worth 1/2 tokens after layer 2: Plug-and-play inference acceleration for large vision-language models. In *European Conference on Computer Vision*, pp. 19–35. Springer, 2024b.

Chen, L., Zhao, H., Liu, T., Bai, S., Lin, J., Zhou, C., and Chang, B. An image is worth 1/2 tokens after layer 2: Plug-and-play inference acceleration for large vision-language models. In *European Conference on Computer Vision*, pp. 19–35. Springer, 2025.

Dai, W., Li, J., Li, D., Tiong, A. M. H., Zhao, J., Wang, W., Li, B., Fung, P., and Hoi, S. InstructBLIP: Towards General-purpose Vision-Language Models with Instruction Tuning, 2023.

Dao, T. Flashattention-2: Faster attention with better parallelism and work partitioning. *ICLR*, 2024.

Dhouib, M., Buscaldi, D., Vanier, S., and Shabou, A. Pact: Pruning and clustering-based token reduction for faster visual language models. In *Proceedings of the Computer Vision and Pattern Recognition Conference*, pp. 14582–14592, 2025.

Ding, L., Zhao, A., Ye, F., Chen, Z., and Shen, X. From llms to lrms: Rethinking pruning for reasoning-centric models. *arXiv preprint arXiv:2601.18091*, 2026.

Eliopoulos, N. J., Jajal, P., Davis, J. C., Liu, G., Thiravathukal, G. K., and Lu, Y.-H. Pruning one more token is enough: Leveraging latency-workload non-linearities for vision transformers on the edge. In *2025 IEEE/CVF Winter Conference on Applications of Computer Vision (WACV)*, pp. 7153–7162. IEEE, 2025.

Fan, Y., Zhao, A., Fu, J., Tong, J., Su, H., Pan, Y., Zhang, W., and Shen, X. Visipruner: Decoding discontinuous cross-modal dynamics for efficient multimodal llms. In *Proceedings of the 2025 Conference on Empirical Methods in Natural Language Processing*, pp. 18896–18913, 2025.

Fernandez, J., Kahn, J., Na, C., Bisk, Y., and Strubell, E. The framework tax: Disparities between inference efficiency in NLP research and deployment. In Bouamor, H., Pino, J., and Bali, K. (eds.), *Proceedings of the 2023 Conference on Empirical Methods in Natural Language Processing*, pp. 1588–1600, Singapore, December 2023.

Fu, C., Chen, P., Shen, Y., Qin, Y., Zhang, M., Lin, X., Yang, J., Zheng, X., Li, K., Sun, X., et al. Mme: A comprehensive evaluation benchmark for multimodal large language models. *arXiv preprint arXiv:2306.13394*, 2023.

Goyal, Y., Khot, T., Summers-Stay, D., Batra, D., and Parikh, D. Making the v in vqa matter: Elevating the role of image understanding in visual question answering. In *Proceedings of the IEEE conference on computer vision and pattern recognition*, pp. 6904–6913, 2017.

Han, C., Liang, Y., Xuan, Z., Wu, D., Zhang, W., and Shen, X. Informed routing in llms: Smarter token-level computation for faster inference. *arXiv preprint arXiv:2510.13831*, 2025.

Han, Y., Liu, X., Zhang, Z., Ding, P., Chen, J., Wang, D., Chen, H., Yan, Q., and Huang, S. Filter, correlate, compress: Training-free token reduction for mllm acceleration. *arXiv preprint arXiv:2411.17686*, 2024.

Huang, W., Zhai, Z., Shen, Y., Cao, S., Zhao, F., Xu, X., Ye, Z., Hu, Y., and Lin, S. Dynamic-llava: Efficient multimodal large language models via dynamic vision-language context sparsification. *arXiv preprint arXiv:2412.00876*, 2024.

Hudson, D. A. and Manning, C. D. Gqa: A new dataset for real-world visual reasoning and compositional question answering. In *Proceedings of the IEEE/CVF conference on computer vision and pattern recognition*, pp. 6700–6709, 2019.

Jiang, P., Li, H., Zhao, L., Chao, F., Yan, K., Ding, S., and Ji, R. Visa: Group-wise visual token selection and aggregation via graph summarization for efficient mllms inference. In *Proceedings of the 33rd ACM International Conference on Multimedia*, pp. 11130–11139, 2025.

Kim, Y., Zhang, Y., Liu, H., Jung, A., Lee, S., and Hong, S. Training-free token pruning via zeroth-order gradient estimation in vision-language models. *arXiv preprint arXiv:2509.24837*, 2025.

Langley, P. Crafting papers on machine learning. In Langley, P. (ed.), *Proceedings of the 17th International Conference on Machine Learning (ICML 2000)*, pp. 1207–1216, Stanford, CA, 2000. Morgan Kaufmann.

Li, B., Ge, Y., Ge, Y., Wang, G., Wang, R., Zhang, R., and Shan, Y. Seed-bench: Benchmarking multimodal large language models. In *Proceedings of the IEEE/CVF Conference on Computer Vision and Pattern Recognition (CVPR)*, pp. 13299–13308, 2024a.

Li, B., Zhang, Y., Guo, D., Zhang, R., Li, F., Zhang, H., Zhang, K., Li, Y., Liu, Z., and Li, C. Llava-onevision: Easy visual task transfer. *arXiv preprint arXiv:2408.03326*, 2024b.

Li, H., Zhang, J., Liao, W., Peng, D., Ding, K., and Jin, L. Redundancylens: Revealing and exploiting visual token processing redundancy for efficient decoder-only mllms. *arXiv preprint arXiv:2501.19036*, 2025a.

Li, J., Li, D., Xiong, C., and Hoi, S. BLIP: Bootstrapping Language-Image Pre-training for Unified Vision-Language Understanding and Generation. In *ICML*, 2022.

Li, J., Li, D., Savarese, S., and Hoi, S. BLIP-2: Bootstrapping language-image pre-training with frozen image encoders and large language models. In *ICML*, 2023a.

Li, W., Yuan, Y., Liu, J., Tang, D., Wang, S., Qin, J., Zhu, J., and Zhang, L. Tokenpacker: Efficient visual projector for multimodal llm. *International Journal of Computer Vision*, pp. 1–19, 2025b.

Li, Y., Du, Y., Zhou, K., Wang, J., Zhao, X., and Wen, J.-R. Evaluating object hallucination in large vision-language models. In *Proceedings of the 2023 Conference on Empirical Methods in Natural Language Processing*, pp. 292–305, 2023b.

Lin, J., Chen, H., Zhu, D., and Shen, X. To preserve or to compress: An in-depth study of connector selection in multimodal large language models. In *Proceedings of the 2024 Conference on Empirical Methods in Natural Language Processing*, pp. 5666–5680, 2024a.

Lin, J., Yin, H., Ping, W., Molchanov, P., Shoeybi, M., and Han, S. Vila: On pre-training for visual language models. In *Proceedings of the IEEE/CVF Conference on Computer Vision and Pattern Recognition*, pp. 26689–26699, 2024b.

Lin, Z., Lin, M., Lin, L., and Ji, R. Boosting multimodal large language models with visual tokens withdrawal for rapid inference. In *Proceedings of the AAAI Conference on Artificial Intelligence*, pp. 5334–5342, 2025.

Liu, A., Tan, R., Gong, B., and Plummer, B. A. Fine-grained token allocation via operation pruning for efficient mllms. *arXiv preprint arXiv:2507.02909*, 2025a.

Liu, H., Li, C., Li, Y., and Lee, Y. J. Improved baselines with visual instruction tuning, 2023a.

Liu, H., Li, C., Wu, Q., and Lee, Y. J. Visual instruction tuning, 2023b.

Liu, H., Li, C., Li, Y., and Lee, Y. J. Improved baselines with visual instruction tuning. In *Proceedings of the IEEE/CVF conference on computer vision and pattern recognition*, pp. 26296–26306, 2024a.

Liu, H., Li, C., Li, Y., Li, B., Zhang, Y., Shen, S., and Lee, Y. J. Llava-next: Improved reasoning, ocr, and world knowledge, January 2024b. URL <https://llava-vl.github.io/blog/2024-01-30-llava-next/>.

Liu, J., Du, F., Zhu, G., Lian, N., Li, J., and Chen, B. Hiprun: Training-free visual token pruning via hierarchical attention in vision-language models. *arXiv preprint arXiv:2508.00553*, 2025b.

Liu, Y., Duan, H., Zhang, Y., Li, B., Zhang, S., Zhao, W., Yuan, Y., Wang, J., He, C., Liu, Z., Chen, K., and Lin, D. Mmbench: Is your multi-modal model an all-around player? In *European conference on computer vision*, pp. 216–233, 2025c.

Lu, P., Mishra, S., Xia, T., Qiu, L., Chang, K.-W., Zhu, S.-C., Tafjord, O., Clark, P., and Kalyan, A. Learn to explain: Multimodal reasoning via thought chains for

science question answering. *Advances in Neural Information Processing Systems*, 35:2507–2521, 2022.

NVIDIA. Gpu performance background user’s guide. <https://docs.nvidia.com/deeplearning/performance/dl-performance-gpu-background/index.html>, 2023.

OpenAI. Introducing chatgpt. <https://openai.com/blog/chatgpt>, 2022.

OpenAI. GPT-4V(ision) System Card, 2023.

OpenGVLab. InternVL2: Better than the Best – Expanding Performance Boundaries of Open-Source Multimodal Models with the Progressive Scaling Strategy, 2024.

Qiu, X., Tong, J., Sun, Y., Ma, Y., and Shen, X. The few govern the many: Unveiling few-layer dominance for time series models. *arXiv preprint arXiv:2511.07237*, 2025.

Shang, Y., Cai, M., Xu, B., Lee, Y. J., and Yan, Y. Llava-prumerge: Adaptive token reduction for efficient large multimodal models. In *Proceedings of the IEEE/CVF International Conference on Computer Vision*, pp. 22857–22867, 2025.

Shao, Z., Wang, M., Yu, Z., Pan, W., Yang, Y., Wei, T., Zhang, H., Mao, N., Chen, W., and Yu, J. Growing a twig to accelerate large vision-language models. *arXiv preprint arXiv:2503.14075*, 2025.

Singh, A., Natarajan, V., Shah, M., Jiang, Y., Chen, X., Batra, D., Parikh, D., and Rohrbach, M. Towards vqa models that can read. In *Proceedings of the IEEE/CVF Conference on Computer Vision and Pattern Recognition (CVPR)*, pp. 8317–8326, 2019.

Song, D., Wang, W., Chen, S., Wang, X., Guan, M. X., and Wang, B. Less is more: A simple yet effective token reduction method for efficient multi-modal llms. In *Proceedings of the 31st International Conference on Computational Linguistics*, pp. 7614–7623, 2025.

Su, H., Zhou, X., Yu, H., Shen, X., Chen, Y., Zhu, Z., Yu, Y., and Zhou, J. Welm: A well-read pre-trained language model for chinese. *arXiv preprint arXiv:2209.10372*, 2022.

Su, H., Tian, Z., Shen, X., and Cai, X. Unraveling the mystery of scaling laws: Part i. *arXiv preprint arXiv:2403.06563*, 2024.

Sun, Y., Xin, Y., Li, H., Sun, J., Lin, C., and Batista-Navarro, R. T. Lvpruning: An effective yet simple language-guided vision token pruning approach for multi-modal large language models. In *Findings of the Association for Computational Linguistics: NAACL 2025*, pp. 4299–4308, 2025.

Tan, X., Ye, P., Tu, C., Cao, J., Yang, Y., Zhang, L., Zhou, D., and Chen, T. Tokencarve: Information-preserving visual token compression in multimodal large language models. *arXiv preprint arXiv:2503.10501*, 2025.

Tong, J., Jin, W., Qin, P., Li, A., Zou, Y., Li, Y., Li, Y., and Li, R. Flowcut: Rethinking redundancy via information flow for efficient vision-language models. *arXiv preprint arXiv:2505.19536*, 2025.

Touvron, H., Lavril, T., Izacard, G., Martinet, X., Lachaux, M.-A., Lacroix, T., Rozière, B., Goyal, N., Hambro, E., Azhar, F., et al. Llama: Open and efficient foundation language models. *arXiv preprint arXiv:2302.13971*, 2023.

Wang, P., Bai, S., Tan, S., Wang, S., Fan, Z., Bai, J., Chen, K., Liu, X., Wang, J., Ge, W., et al. Qwen2-vl: Enhancing vision-language model’s perception of the world at any resolution. *arXiv preprint arXiv:2409.12191*, 2024.

Wang, W., Gao, Z., Gu, L., Pu, H., Cui, L., Wei, X., Liu, Z., Jing, L., Ye, S., Shao, J., et al. Internvl3. 5: Advancing open-source multimodal models in versatility, reasoning, and efficiency. *arXiv preprint arXiv:2508.18265*, 2025.

Wen, Z., Gao, Y., Li, W., He, C., and Zhang, L. Token pruning in multimodal large language models: Are we solving the right problem? In Che, W., Nabende, J., Shutova, E., and Pilehvar, M. T. (eds.), *Findings of the Association for Computational Linguistics: ACL 2025*, pp. 15537–15549, Vienna, Austria, July 2025a.

Wen, Z., Gao, Y., Wang, S., Zhang, J., Zhang, Q., Li, W., He, C., and Zhang, L. Stop looking for important tokens in multimodal language models: Duplication matters more. *arXiv preprint arXiv:2502.11494*, 2025b.

Wu, Q., Xu, W., Liu, W., Tan, T., Liu, J., Li, A., Luan, J., Wang, B., and Shang, S. Mobilevlm: A vision-language model for better intra-and inter-ui understanding. *arXiv preprint arXiv:2409.14818*, 2024.

Xing, L., Huang, Q., Dong, X., Lu, J., Zhang, P., Zang, Y., Cao, Y., He, C., Wang, J., Wu, F., et al. Pyramid-drop: Accelerating your large vision-language models via pyramid visual redundancy reduction. *arXiv preprint arXiv:2410.17247*, 2024a.

Xing, L., Huang, Q., Dong, X., Lu, J., Zhang, P., Zang, Y., Cao, Y., He, C., Wang, J., Wu, F., et al. Pyramid-drop: Accelerating your large vision-language models via pyramid visual redundancy reduction. *arXiv preprint arXiv:2410.17247*, 2024b.

Yang, S., Chen, Y., Tian, Z., Wang, C., Li, J., Yu, B., and Jia, J. Visionzip: Longer is better but not necessary in vision language models. In *Proceedings of the Computer Vision and Pattern Recognition Conference*, pp. 19792–19802, 2025a.

Yang, S., Xu, R., Cui, C., Wang, T., Lin, D., and Pang, J. Vflowopt: A token pruning framework for lmms with visual information flow-guided optimization. In *Proceedings of the IEEE/CVF International Conference on Computer Vision*, pp. 23924–23934, 2025b.

Ye, W., Wu, Q., Lin, W., and Zhou, Y. Fit and prune: Fast and training-free visual token pruning for multimodal large language models. In *Proceedings of the AAAI Conference on Artificial Intelligence*, pp. 22128–22136, 2025a.

Ye, X., Gan, Y., Ge, Y., Zhang, X.-P., and Tang, Y. Atp-llava: Adaptive token pruning for large vision language models. In *Proceedings of the Computer Vision and Pattern Recognition Conference*, pp. 24972–24982, 2025b.

Yin, H., Si, G., and Wang, Z. Lifting the veil on visual information flow in mllms: Unlocking pathways to faster inference. In *Proceedings of the Computer Vision and Pattern Recognition Conference*, pp. 9382–9391, 2025.

Yuan, Q., Zhang, Q., Liu, Y., Chen, J., Lu, Y., Lin, H., Zheng, J., Han, X., and Sun, L. Shortv: Efficient multimodal large language models by freezing visual tokens in ineffective layers. *arXiv preprint arXiv:2504.00502*, 2025.

Zamini, M. and Shukla, D. Delta-llava: Base-then-specialize alignment for token-efficient vision-language models. *arXiv preprint arXiv:2512.18910*, 2025.

Zeng, W., Huang, Z., Ji, K., and Yan, Y. Skip-vision: Efficient and scalable acceleration of vision-language models via adaptive token skipping. *arXiv preprint arXiv:2503.21817*, 2025.

Zhang, C., Ma, K., Fang, T., Yu, W., Zhang, H., Zhang, Z., Xie, Y., Sycara, K., Mi, H., and Yu, D. Vscan: Rethinking visual token reduction for efficient large vision-language models. *arXiv preprint arXiv:2505.22654*, 2025a.

Zhang, E., Yu, F., Wu, A., Wen, Z., Yan, K., Ding, S., Qi, B., and Zhang, L. D2pruner: Debiased importance and structural diversity for mllm token pruning. *arXiv preprint arXiv:2512.19443*, 2025b.

Zhang, Q., Cheng, A., Lu, M., Zhang, R., Zhuo, Z., Cao, J., Guo, S., She, Q., and Zhang, S. Beyond text-visual attention: Exploiting visual cues for effective token pruning in vlms. *arXiv preprint arXiv:2412.01818*, 2025c.

Zhang, Q., Liu, M., Li, L., Lu, M., Zhang, Y., Pan, J., She, Q., and Zhang, S. Beyond attention or similarity: Maximizing conditional diversity for token pruning in mllms. *arXiv preprint arXiv:2506.10967*, 2025d.

Zhang, Y., Fan, C.-K., Ma, J., Zheng, W., Huang, T., Cheng, K., Gudovskiy, D., Okuno, T., Nakata, Y., Keutzer, K., et al. Sparsevlm: Visual token sparsification for efficient vision-language model inference. In *International Conference on Machine Learning*, 2025e.

Zhang, Z., Pham, P., Zhao, W., Wan, K., Li, Y.-J., Zhou, J., Miranda, D., Kale, A., and Xu, C. Treat visual tokens as text? but your mllm only needs fewer efforts to see. *arXiv preprint arXiv:2410.06169*, 2024.

Zhang, Z., Yadav, S., Han, F., and Shutova, E. Cross-modal information flow in multimodal large language models. In *Proceedings of the Computer Vision and Pattern Recognition Conference*, pp. 19781–19791, 2025f.

Zhang, Z., Yadav, S., Han, F., and Shutova, E. Cross-modal information flow in multimodal large language models. In *Proceedings of the Computer Vision and Pattern Recognition Conference*, pp. 19781–19791, 2025g.

Zhao, A., Ye, F., Fan, Y., Tong, J., Fei, Z., Su, H., and Shen, X. Skipgpt: Dynamic layer pruning reinvented with token awareness and module decoupling. *arXiv preprint arXiv:2506.04179*, 2025a.

Zhao, W., Han, Y., Tang, J., Li, Z., Song, Y., Wang, K., Wang, Z., and You, Y. A stitch in time saves nine: Small vlm is a precise guidance for accelerating large vlms. In *Proceedings of the Computer Vision and Pattern Recognition Conference*, pp. 19814–19824, 2025b.

Zheng, L., Chiang, W.-L., Sheng, Y., Zhuang, S., Wu, Z., Zhuang, Y., Lin, Z., Li, Z., Li, D., Xing, E., et al. Judging llm-as-a-judge with mt-bench and chatbot arena. *Advances in neural information processing systems*, 36: 46595–46623, 2023.

Zou, X., Lu, D., Wang, Y., Yan, Y., Lyu, Y., Zheng, X., Zhang, L., and Hu, X. “Don’t just chase” highlighted tokens” in mllms: Revisiting visual holistic context retention. *arXiv preprint arXiv:2510.02912*, 2025.

To complement the manuscript, this appendix presents additional content and is organized as follows:

- Section. A: presents additional experimental results.
- Section. B: provides extended analyses of layerwise redundancy across different model components, including attention and feed-forward modules, and across model scales.
- Section. C: details implementation and efficiency-related aspects.
- Section. D: describes the comparison methods.
- Section. E: introduces the benchmarks.

A. Additional Results

To assess cross-scale generalization, we report results on LLaVA-1.5-3B and LLaVA-1.5-13B in Table 7, comparing our method with representative training-free and training-based pruning approaches. On LLaVA-1.5-3B, our method preserves 98.7% of baseline accuracy while reducing vision-side computation to 4.5%, which can be further lowered to 2.0% when combined with PyramidDrop at inference time. On LLaVA-1.5-13B, it achieves 97.0% relative accuracy using only 3.3% of the original visual computation, further reduced to 1.7% with PyramidDrop. These results demonstrate that the proposed ViCA generalizes well across model scales, consistently achieving a strong accuracy-efficiency trade-off.

Table 7. Performance comparison of different pruning approaches on LLaVA-1.5-3B and LLaVA-1.5-13B across nine benchmarks. Methods are grouped by pruning strategy: no background color indicates training-free methods, red denotes training-based pruning, and blue highlights our approach. ViCA refers to the model retrained under the proposed minimal efficient architecture using the standard two-stage pretraining and fine-tuning pipeline. ViCA+PDrop[†] further applies PyramidDrop at inference time. Op and Tok denote operation-level and token-level pruning methods, respectively. Vision-related computation and token counts are measured following the FLOPs formulation in Appendix C.3.

Method	Sparsity Op.	Tok.	Vision-side TFLOPs (Rel.)		MME ^P	MMB	MMB ^{CN}	GQA	VQA ^{v2}	SQA ^I	VQA ^{Text}	POPE	SEED ^I	Rel. Avg.
LLaVA-1.5-3B														
Original	-	-	576	3.04 (100.0%)	1258.2	57.0	28.6	59.4	75.3	60.0	48.6	86.4	60.1	100.0%
PDrop		✓	270	1.40 (46.0%)	1231.1	54.3	29.0	57.0	72.9	60.3	48.7	87.1	61.4	97.0%
YOPO	✓		70	0.37 (12.0%)	1106.5	48.6	29.0	50.4	64.3	56.5	39.6	83.7	51.4	89.2%
ViCA	✓		27	0.14 (4.5%)	1188.9	55.4	33.2	56.6	72.1	61.2	45.4	86.2	56.7	98.7%
ViCA+PDrop [†]	✓	✓	12	0.06 (2.0%)	1187.5	56.3	34.5	54.8	71.1	60.8	44.8	84.3	55.2	98.2%
LLaVA-1.5-13B														
Original	-	-	576	14.91 (100.0%)	1529.9	68.5	63.5	63.3	80.0	72.8	61.2	87.0	68.2	100.0%
FastV		✓	64	1.63 (10.9%)	1246.4	59.2	55.1	51.9	65.3	73.1	53.4	56.9	56.1	83.7%
ToMe	✓		64	1.63 (10.9%)	1287.0	59.5	51.4	55.3	67.1	70.7	50.1	71.5	-	85.5%
PDrop	✓		64	1.63 (10.9%)	1247.0	63.1	56.6	54.1	70.8	73.1	55.3	66.1	58.4	87.7%
HiPrune	✓		64	1.63 (10.9%)	-	64.8	59.2	54.2	70.3	74.6	56.7	72.4	-	91.4%
SparseVLM	✓		64	1.63 (10.9%)	1374.3	65.2	60.3	55.9	73.2	73.0	57.1	77.9	60.3	92.4%
VISA	✓		64	1.63 (10.9%)	1468.3	66.0	60.3	57.4	75.5	73.9	59.2	79.5	-	95.3%
VisionZip	✓		32	0.81 (5.5%)	1257.7	61.2	55.8	52.7	68.4	72.9	55.2	66.8	56.2	86.4%
DART	✓		32	0.81 (5.5%)	1282.8	61.9	56.2	53.9	68.1	73.2	55.1	66.9	57.6	87.2%
VisPruner	✓		32	0.81 (5.5%)	1314.2	61.3	56.1	52.6	69.0	71.7	56.0	71.9	56.5	87.6%
DivPrune	✓		32	0.81 (5.5%)	1405.2	61.7	57.2	56.2	72.0	70.9	54.6	79.3	60.1	90.7%
DOP _V	✓	✓	32	0.81 (5.5%)	1365.6	64.3	59.5	56.0	73.2	73.6	57.2	78.8	59.7	92.2%
CDPruner	✓		32	0.81 (5.5%)	1421.0	63.7	56.6	58.5	75.2	71.9	55.3	87.6	62.5	93.7%
DOP _{CD}	✓	✓	32	0.81 (5.5%)	1468.9	65.1	58.7	59.0	76.2	68.9	56.7	87.5	63.8	94.8%
PDrop	✓		270	6.92 (46.4%)	1555.2	68.8	63.6	63.1	79.6	70.9	60.8	87.6	68.1	99.8%
Delta-LLaVA	✓		144	3.68 (24.7%)	1527.5	67.4	-	62.7	76.9	71.6	59.2	87.3	-	98.4%
Dynamic-LLaVA	✓		115	2.93 (19.7%)	1554.1	68.3	-	62.7	79.1	72.2	59.5	86.8	66.6	99.1%
YOPO	✓		70	1.78 (12.0%)	1430.0	66.2	60.6	61.2	78.1	70.7	56.7	86.4	65.4	96.1%
VisionZip	✓		64	1.63 (10.9%)	-	65.5	-	58.1	75.2	72.3	58.5	81.8	61.4	94.4%
TwigVLM	✓		64	1.63 (10.9%)	1503.1	66.2	61.1	62.5	77.2	73.6	59.5	84.1	63.2	97.1%
LLaVA-PruMerge	✓		32	0.81 (5.5%)	1428.6	62.3	54.5	53.3	72.8	71.0	58.4	78.5	54.4	89.8%
TRIM	✓		29	0.74 (4.9%)	1337.9	65.5	52.4	56.0	75.4	70.1	50.7	85.2	60.8	90.5%
ViCA	✓		19	0.49 (3.3%)	1453.6	67.1	62.3	61.8	77.9	72.2	56.7	86.5	65.2	97.0%
ViCA+PDrop [†]	✓	✓	10	0.26 (1.7%)	1442.1	65.7	62.7	60.7	77.4	72.1	56.8	85.9	64.7	96.3%

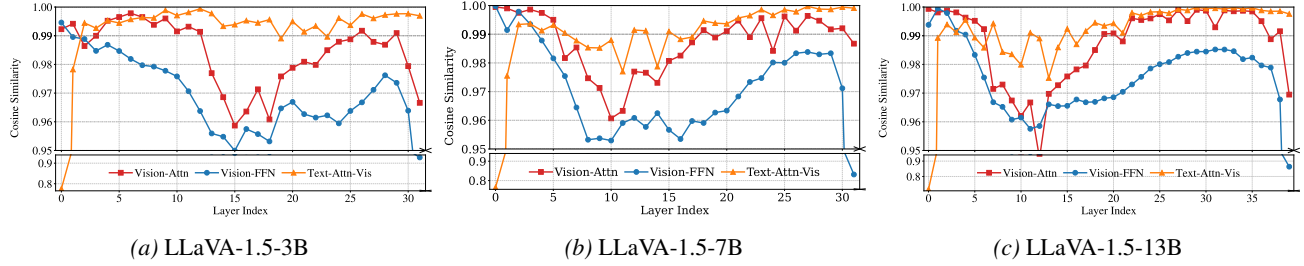


Figure 6. Token-wise mean cosine similarity on TextVQA (Singh et al., 2019) before and after key modules across LLaVA-1.5-3B, 7B, and 13B. *Vision-Attn* measures vision token similarity before and after attention, *Vision-FFN* measures vision token similarity before and after FFN, and *Text-Attn-Vis* measures text-token similarity before and after text–vision cross-attention.

B. More Models Analysis

B.1. Layerwise Redundancy in Text-to-Vision Cross-Attention

We compute the cosine similarity of text-token representations before and after vision-to-text cross-attention at each layer to identify critical text-to-vision cross-attention layers. As shown in Fig. 6, *Text-Attn-Vis* represents the cosine similarity of text tokens before and after *text–vision* cross-attention. The similarity is lowest in the shallow layers (0–1), indicating that visual information is integrated into text representations early. A secondary dip occurs in the middle layers (7–11 and 14), suggesting further text–vision fusion. These shallow and middle layers (0–1, 7–11, and 14) thus serve as the primary stages of text–vision interaction. Beyond these layers, the similarity increases significantly, indicating that the influence of visual information on text representations diminishes.

We further conduct *training-free masking* experiments, summarized in Table 8. Masking all text-to-vision cross-attention layers causes a 53.8% drop in performance across nine benchmarks. In contrast, retaining text-to-vision cross-attention only in the selected shallow and middle layers (0–1, 7–11, and 14) limits the performance drop to 6.5%, while masking cross-attention in these layers results in a much larger drop of 37.0%. These results indicate that text-to-vision cross-attention is essential for visual fusion, but its effect is concentrated in the key layers mentioned above, with the remaining layers contributing marginally to final multimodal reasoning.

Building on these results, we validate the findings under *retraining*, as shown in Table 8. Enabling text-to-vision cross-attention only in the selected shallow and middle layers (0–1, 7–11, and 14) restores 99.5% of the baseline performance on average. Adding a low-similarity layer (16) further improves performance, slightly surpassing the baseline at 100.5%. These findings demonstrate that preserving text-to-vision cross-attention only in the essential shallow and middle layers is sufficient to recover the original performance.

Finding 1: Multimodal reasoning depends on only a small number of *text-to-vision cross-attention* layers that inject visual information into text tokens.

B.2. Layerwise Redundancy in Attention-Based Vision Updates

After analyzing text-to-vision cross-attention, we investigate the dynamics of visual representations by computing the cosine similarity of vision token representations before and after the attention module at each layer. As shown in Fig. 6, *Vision-Attn* exhibits lower similarity in the middle layers (6–17), indicating continuous changes in visual representations. However, since text-to-vision cross-attention is mainly concentrated in layers 7–11, vision updates in layers 12–17 are less likely to influence text tokens through cross-modal pathways, thus having a limited impact on final predictions.

To verify this, we perform *training-free masking* experiments, as shown in Table 8. Masking all *vision update attention* operations results in a 9.3% performance drop. Retaining updates in layers 6–17 reduces the drop to 1.2%, while restricting them to layers 6–11 yields a similar drop. In contrast, masking updates in layers 6–11 alone causes a larger drop of 4.7%. Overall, compared to text-to-vision cross-attention, attention-based updates on vision tokens contribute much less to performance, with layers 6–11 being relatively more important.

Finally, we validate this conclusion by retraining the model. In the training-free setting, masking all attention-based vision

Table 8. Redundancy diagnosis for identifying and validating candidate key layers of vision-related operations in LLaVA-1.5-7B. Step 1 measures cosine similarity between tokens before and after the target operations to identify candidate key layers. In Step 2, we perform training-free verification by retaining only the critical layers and comparing against retaining only the remaining non-critical layers and masking all layers. Step 3 conducts retraining experiments comparing models retaining only the key layers to those removing all layers.

Setup	Retained Layers	Layer Indices	MME ^P	MMB	MMB ^{CN}	GQA	VQA ^{v2}	SQA ^I	VQA ^T	POPE	SEED ^I	Avg(%)
Baseline												
-	Full	0-31	1506.5	64.7	58.1	61.9	78.5	69.5	58.2	86.8	66.2	100.0
Text–Vision Cross-Attention												
Diagnosis	Lowest cosine similarity at layers 0–1, 7–11, and 14 (16 as extension).											
Training-free	Essential	0–1,7–11,14	1393.5	62.5	55.9	54.4	66.7	68.6	51.3	86.1	64.4	93.5
Training-free	Non-essential	2–6,12–13,15–31	758.2	24.9	17.4	44.8	-	61.0	45.5	70.4	43.4	63.0
	Frozen	-	572.1	16.0	11.3	29.9	34.0	56.5	29.9	50.3	34.2	46.2
Training	Essential	0–1, 7–11, 14	1476.6	66.1	58.3	62.7	77.9	67.5	56.4	87.1	66.0	99.5
	Essential (expanded)	0–1, 7–11, 14, 16	1463.7	69.3	59.1	62.7	78.2	68.6	56.9	87.1	66.6	100.5
vision update Attention												
Diagnosis	Lowest cosine similarity at layers 6–17. Considering overlap with text–vision fusion, layers 6–11 are identified as key layers.											
Training-free	Over-approx.	6–17	1469.7	64.7	57.1	61.6	78.1	68.5	56.6	86.0	65.6	98.8
Training-free	Essential	6–11	1454.5	64.4	57.1	61.0	77.1	68.6	56.1	86.7	65.5	98.3
Training-free	Non-essential	0–5,12–31	1361.2	61.3	55.7	59.2	-	68.8	55.4	83.9	62.9	95.3
	Frozen	-	1298.2	62.5	54.2	54.5	70.4	69.0	51.0	79.8	61.0	91.7
Training	Frozen	-	1501.1	66.1	59.5	62.1	78.0	69.3	57.1	87.1	65.8	100.2
vision update FFN												
Diagnosis	Lowest similarity at layers 5–31. Considering overlap with text–vision fusion, layers 5–11 are identified as key layers.											
Training-free	Essential	5–11	1463.2	64.5	55.2	58.9	74.6	68.7	54.2	85.2	65.3	96.8
Training-free	Non-essential	0–4,12–31	988.6	56.9	47.8	49.8	-	66.3	48.9	65.4	55.2	81.8
	Frozen	-	876.8	52.0	38.8	39.6	45.2	66.3	40.9	61.1	51.6	71.2
Training	Essential	5–11	1475.7	66.7	58.4	63.3	78.7	68.4	58.2	87.3	66.9	100.5
	Essential(aggressive)	5,7,9	1493.5	67.4	57.7	62.3	78.0	70.8	57.9	87.4	65.8	100.5
	Frozen	-	1472.4	65.6	56.9	62.0	77.5	70.3	56.9	87.3	64.6	99.2

updates causes a smaller drop than masking text–vision cross-attention. Based on this observation, and noting that *vision self-attention* accounts for most of the attention computation, we remove all attention operations that update vision tokens and retrain the model. As shown in Table 8, the retrained model achieves 100.2% of baseline performance across nine benchmarks, indicating that attention-based vision updates are functionally ineffective. This suggests that vision-related quadratic computation can be safely reduced to linear scale.

Finding 2: Attention-based vision updates in later layers have limited impact on final predictions, and vision-related quadratic computations can be safely reduced to linear scale without significant performance loss.

B.3. Layerwise Redundancy in FFN-Based Vision Updates

Since FFNs have a large expansion dimension, they are the primary linear component of vision-side computation, with detailed FLOPs derivations provided in Appendix C.3. In MLLMs, FFNs primarily refine visual features, while cross-modal information exchange occurs in attention. We hypothesize that FFN updates on vision tokens after the effective text-to-vision cross-attention layers, confined to shallow and middle layers, have limited influence on text representations and final outputs.

To test this hypothesis, we use the same cosine-similarity method to compute the mean similarity of vision token representations before and after the FFN at each layer. As shown in Fig. 6, *Vision-FFN* represents the cosine similarity of vision tokens before and after each FFN layer. The similarity remains low after layer 5, indicating representational changes. Since text-to-vision cross-attention is most active in layers 7 to 11, this suggests that FFN updates in layers 5 to 11 play a significant role in refining visual features. Updates in deeper layers are less likely to influence text tokens and final outputs.

We conduct *training-free pruning* experiments by skipping FFN computation on vision tokens in selected layers. As shown in Table 8, skipping FFNs across all layers results in a 28.8% performance drop. In contrast, retaining FFNs only in layers 5 to 11 reduces the drop to 3.2%. Skipping FFNs in layers 5 to 11 results in an 18.2% drop. This indicates that only a small subset of FFN layers is necessary for vision token updates.

Finally, we validate these observations by retraining the model. In the retraining process, vision tokens skip FFN computation in selected layers, and we evaluate the model on nine benchmarks. As reported in Table 8, skipping all FFN layers for vision tokens still preserves 99.2% of the baseline performance. Enabling FFNs only in layers 5 to 11, or selectively in layers 5, 7, and 9, both reaches 100.5% of the baseline.

Finding 3: Skipping all FFN updates on vision tokens, even after retraining, still preserves near-baseline performance, indicating that only a small subset of FFN layers is crucial for vision token updates.

B.4. Redundancy Diagnosis Across Model Scales

Table 9. Redundancy diagnosis for identifying and validating candidate key layers of vision-related operations in LLaVA-1.5-13B. Step 1 measures cosine similarity using token before and after the target operations to identify candidate key layers. Step 2 performs a training-free verification by retaining candidate key layers and comparing with masking all layers.

Setup	Retained Layers	Layer Indices	MME ^P	MMB	MMB ^{CN}	GQA	VQA ^{v2}	SQA ^I	VQA ^T	POPE	SEED ^I	Avg(%)
Baseline												
-	Full	0–31	1529.9	68.5	63.5	63.3	80.0	72.8	61.2	87.0	68.2	100.0
Text–Vision Cross-Attention												
Diagnosis	Lowest similarity at layers 0, 6, 8–10, 13–14, and 16.											
Training-free	Essential	0,6,8–10,13–14,16	1362.8	66.4	61.7	56.8	–	71.3	55.3	–	66.8	94.2
	Frozen	–	673.3	15.4	–	26.7	69.5	56.5	22.9	50.6	33.1	52.1
vision update Attention												
Diagnosis	Lowest similarity at layers 7–18. Considering overlap with text–vision fusion, layers 7–14 are identified as key layers.											
Training-free	Over-approx.	7–18	1461.1	68.0	62.8	62.6	79.3	71.9	59.5	85.7	67.7	98.4
	Essential	7–14	1464.4	68.1	62.6	62.2	79.0	71.9	59.5	86.1	67.6	98.3
	Frozen	–	1246.1	63.9	55.0	54.8	69.5	69.1	47.8	87.2	63.4	89.0
vision update FFN												
Diagnosis	Lowest similarity at layers 5–39. Considering overlap with text–vision fusion, layers 5–14 are identified as key layers.											
Training-free	Essential	5–14	1505.0	68.8	62.6	62.6	79.1	72.6	59.5	87.2	67.8	99.1
	Frozen	–	969.5	61.3	52.9	49.2	54.3	71.3	48.9	57.6	57.9	79.0

The findings above are first established on LLaVA-1.5-7B. To examine whether these redundancy patterns generalize across different model scales, we apply the same layerwise redundancy diagnosis to LLaVA-1.5-3B and LLaVA-1.5-13B, assessing whether the pruning strategy developed for 7B can be transferred to these models.

We present the layerwise cosine-similarity curves for LLaVA-1.5-3B and 13B in Fig. 6, respectively, analyzing the same three components: (i) text-to-vision cross-attention, (ii) vision update attention, and (iii) vision update FFN.

For text-to-vision cross-attention, low-similarity layers are observed at $\{0–1, 14–15, 18–19, 21–23\}$ in LLaVA-1.5-3B and at $\{0, 6, 8–10, 13–14, 16\}$ in LLaVA-1.5-13B. Training-free masking experiments (Tab. 9, Tab. 10) show that retaining only these candidate key layers preserves 87.1% and 94.2% of the original average accuracy for 3B and 13B, respectively.

The cosine-similarity curves of vision update attention exhibit broad low-similarity regions (3B: $\{2–3, 13–31\}$; 13B: $\{7–18\}$). When aligned with the effective text-to-vision cross-attention window, these regions become substantially narrower. Retaining vision update attention only in the identified key layers preserves 99.3% and 98.3% accuracy for the 3B and 13B models, respectively, while masking all vision update attention leads to degradations of 37.5% and 11.0%, which remain smaller than those caused by removing all text-to-vision cross-attention.

Similarly, vision FFNs exhibit broad low-similarity ranges (3B: $\{3–31\}$; 13B: $\{5–39\}$), but their effective contribution becomes sharply constrained once aligned with the text-to-vision cross-attention window. Training-free pruning shows that enabling FFNs only in the identified layers preserves 101.9% and 99.1% of the average accuracy for the 3B and 13B models, respectively, indicating that only a small subset of FFNs meaningfully contributes to multimodal reasoning. In contrast, skipping all vision FFNs leads to substantially larger performance degradations of 47.2% and 21.0%.

Based on these consistent patterns, we transfer the pruning strategy developed for LLaVA-1.5-7B to the 3B and 13B models with standard pretraining and finetuning. As shown in Sec. 5.3 and Table 6, removing visual token updates in both attention and FFN modules yields the *FreezeVis* variants, which recover 100.3% and 97.4% of the baseline accuracy, respectively.

Table 10. Redundancy diagnosis for identifying and validating key vision-related operations in LLaVA-1.5-3B. Step 1 measures cosine similarity using token before and after the target operations to identify key layers. Step 2 performs a training-free verification by masking non-critical layers and comparing with masking all layers.

Setup	Retained Layers	Layer Indices	MME ^P	MMB	MMB ^{CN}	GQA	SQA ^I	VQA ^T	POPE	SEED ^I	Avg(%)
Baseline											
-	Full	0–31	1258.2	57.0	28.6	59.4	60.0	48.6	86.4	60.1	100.0
Text–Vision Cross-Attention											
Diagnosis											
Training-free	Essential	0–1,14–15,18–19,21–23	1156.0	50.7	18.3	49.5	58.7	41.2	80.3	57.3	87.1
	Frozen	-	558.2	11.0	4.0	31.9	52.9	22.3	49.7	33.4	47.3
vision update Attention											
Diagnosis											
Training-free	Over-approx.	2–3,13–31	1295.9	54.6	31.5	57.6	59.8	45.9	84.7	58.7	99.5
	Essential	2–3,13–23	1293.8	54.7	31.1	57.6	59.8	45.8	84.6	58.9	99.3
	Frozen	-	901.1	18.3	3.2	41.0	53.8	34.6	77.4	39.3	62.5
vision update FFN											
Diagnosis											
Training-free	Essential	3–23	1305.4	57.0	32.9	58.4	61.5	46.9	86.3	59.5	101.9
	Frozen	-	580.3	19.3	5.2	34.6	53.7	28.6	48.5	37.1	52.8

Further restricting visual key–value participation to the identified critical text-to-vision cross-attention layers produces the *ViCA* variants, retaining 98.7% and 97.0% accuracy while reducing vision-related computation to 4.5% and 3.3%. These results demonstrate that the proposed minimal and efficient architecture generalizes consistently across model scales.

C. Implementation Details

C.1. Details of Backbones

Table 11. Model configurations of LLaVA-1.5 backbones.

Model	LLaVA-3B	LLaVA-7B	LLaVA-13B
LLM Backbone	MobileLLaMA-2.7B	Vicuna-7B	Vicuna-13B
Blocks	32	32	40
Heads	32	32	40
Hidden Dim	2560	4096	5120
FFN Dim	6912	11008	13824

C.2. Configuration Details of Our Method

Preserved Text-to-Vision Cross-Attention Layers. Preserved text-to-vision cross-attention layers for each backbone:

- **LLaVA-1.5-3B:** {0, 1, 14, 15, 18, 19, 21, 22, 23}.
- **LLaVA-1.5-7B:** {0, 1, 7, 8, 9, 10, 11, 14}.
- **LLaVA-1.5-13B:** {0, 6, 8, 9, 10, 13, 14, 16}.

Integration of PyramidDrop into Our Method. During inference, our method integrates PyramidDrop, which applies multi-stage vision token dropping for each backbone:

- **LLaVA-1.5-3B:** 25% of vision tokens are dropped at layers 1, 14, and 18.
- **LLaVA-1.5-7B:** 25% of vision tokens are dropped at layers 1, 7, and 10.
- **LLaVA-1.5-13B:** 25% of vision tokens are dropped at layers 6, 9, and 13.

C.3. Details of Calculation Equation of FLOPs

To further explore the computation bottleneck, we refer to the theoretical formulations of vision-related computation proposed in prior works (Chen et al., 2025; Yang et al., 2025a; Liu et al., 2025a; Zhang et al., 2025a), and decompose the vision-related computation in MLLMs into two major components.

Attention Computation. In each attention block, input tokens are first linearly projected into queries, keys, and values, followed by attention multiplications $QK^\top V$ that enable information exchange among tokens. The resulting outputs are then linearly projected by an output projection to produce the final representations of the block.

Among these operations, the visual-related projections include four components— W_K , W_K , W_V , and W_O . Thus, the total cost of visual attention projections is:

$$\mathcal{C}_{\text{Vis-Projector}} = n_{\text{layers}} * 2 * 4nd^2, \quad (1)$$

where n_{layers} is the number of transformer blocks, the factor of 2 converts MACs into FLOPs, and n denotes the number of vision tokens while d denotes the hidden dimension.

During the attention multiplication stage, vision tokens engage in two types of interactions: (i) *vision-to-vision self-attention*, and (ii) *text-vision cross-attention*, with corresponding computational costs:

$$\begin{aligned} \mathcal{C}_{\text{vision-vision}} &= n_{\text{layers}} * 2 * 2dn^2, \\ \mathcal{C}_{\text{text-vision}} &= n_{\text{layers}} * 2 * 2dnt, \end{aligned} \quad (2)$$

where t denote the numbers of text tokens. The total attention multiplication cost about vision tokens is:

$$\mathcal{C}_{V_{is}-QK^\top V} = n_{\text{layers}} * 2 * 2d(n^2 + nt). \quad (3)$$

Accordingly, the total visual-related attention cost can be expressed as:

$$\begin{aligned} \mathcal{C}_{\text{Vis-Attn}} &= \mathcal{C}_{\text{Vis-Projector}} + \mathcal{C}_{V_{is}-QK^\top V} \\ &= n_{\text{layers}} * 2 * (4nd^2 + (2dn^2 + 2dnt)). \end{aligned} \quad (4)$$

FFN Computation. Each Feed-Forward Network (FFN) comprises three main modules: (i) an *up-projection* that expands the hidden dimension from d to m , (ii) a *gating* operation, and (iii) a *down-projection* that maps features back from m to d . Hence, the total cost of a gated FFN is:

$$\mathcal{C}_{\text{Vis-FFN}} = n_{\text{layers}} * 2 * (3ndm), \quad (5)$$

where m denote the expansion dimension. Since $m \gg d$, FFNs constitute the dominant linear component of the overall visual computation.

Total Computation. By combining the attention and FFN costs, the total visual computation can be summarized as:

$$\begin{aligned} \mathcal{C}_{\text{Vis}} &= \mathcal{C}_{\text{Vis-Attn}} + \mathcal{C}_{\text{Vis-FFN}} \\ &= n_{\text{layers}} * 2 * (4nd^2 + 2d(n^2 + nt) + 3ndm). \end{aligned} \quad (6)$$

This formulation clearly shows that the vision self-attention term grows quadratically with the number of vision tokens, while all other terms scale only linearly with n . When $n \ll d$, the quadratic term $2dn^2$ is substantially smaller than the attention projection cost $4nd^2$ and the FFN cost $3ndm$, making the total visual computation scale *near linearly* with the number of vision tokens. Extending this analysis, the total computations is:

$$\mathcal{C}_{\text{Total}} = n_{\text{layers}} * 2 * (4Ld^2 + 2dL^2 + 3Ldm), \quad (7)$$

where $L = n + t$. Here, $4Ld^2$ corresponds to the four projection operations (W_Q , W_K , W_V , W_O) applied to all tokens, $2dL^2$ represents the FLOPs of the $QK^\top V$ attention multiplications across all tokens, and $3Ldm$ denotes the computation of the FFN module for the entire sequence. To further quantify the contribution of visual computation, we examine the ratio between the visual computation and the total FLOPs:

$$\frac{\mathcal{C}_{\text{Vis}}}{\mathcal{C}_{\text{Total}}} = \frac{4nd^2 + 2d(n^2 + nt) + 3ndm}{4Ld^2 + 2dL^2 + 3Ldm}. \quad (8)$$

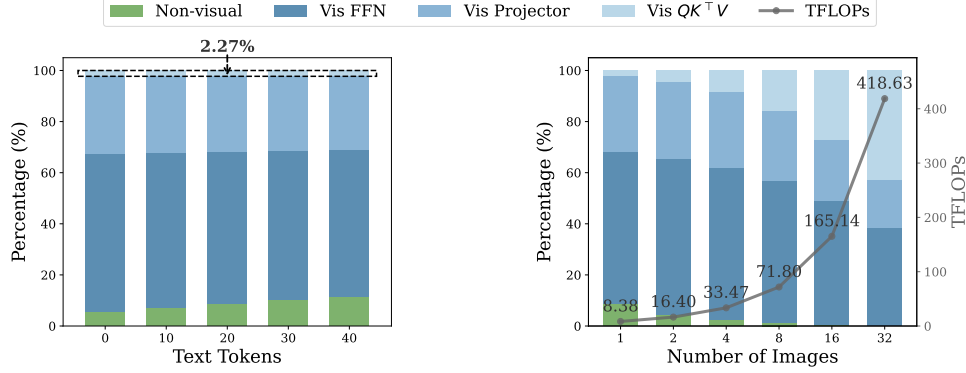


Figure 7. Computation breakdown of LLaVA-1.5-7B across question and vision token scales. *Vis QK^T V*, *Vis Projector*, *Vis FFN*, *Non-Visual*, and *TFLOPs* denote the costs of visual-related attention multiplications, visual attention projections, visual FFN, non-visual computation, and total computation, respectively. Left: *Vis QK^T V* stays at 2.27%.

Equivalent Visual Token Count. To enable fair comparison, we report the *equivalent visual token count* n_{eq} , which is the number of visual tokens that would produce the same vision-side FLOPs in the original model. It is computed as:

$$n_{eq} = \frac{-2n_{layers}(4d^2 + 2dt + 3dm) + \sqrt{[2n_{layers}(4d^2 + 2dt + 3dm)]^2 + 16n_{layers}d\mathcal{C}_{Vis}}}{8n_{layers}d} \quad (9)$$

Case Study on LLaVA-1.5-7B. We further analyze the computational cost in LLaVA-1.5-7B, using representative parameters $n = 576$, $d = 4096$, $m = 11008$, and $n_{layers} = 32$. The number of text tokens t consists of system tokens $t_s = 35$ and question tokens t_t , where t_t typically ranges from 0 to 40 across benchmarks. Among all vision-related components, only the text-to-vision cross-attention in $QK^T V$ attention multiplication depends on the t_t . As illustrated in Fig. 7, as t_t increases from 0 to 40, the proportion of *Vis QK^T V* multiplication in the total computation consistently remains around 2.27%, indicating that variations in question tokens length (from 0 to 40 tokens) have a negligible effect. Therefore, for simplicity, we fix $t_t = 20$ in all subsequent analyses.

In contrast to the negligible effect of text length, the number of vision tokens strongly reshapes the computational profile. As shown in Fig. 7, increasing the image count from 1 to 32 (576 tokens each) shifts the bottleneck from FFN to attention: the visual FFN share drops from 59.49% to 38.12%, visual attention-projector from 29.52% to 18.91%, while visual $QK^T V$ multiplications soar from 2.27% to 42.68%. This marks a clear transition from FFN-dominated to attention-dominated computation as visual token density increases.

Using Eq. (6) and (7), the visual FLOPs of LLaVA-1.5-7B is:

$$\mathcal{C}_{Vis} = n_{layers} \cdot 2(4nd^2 + 2d(n^2 + nt) + 3ndm) \approx 7.65 \text{ TFLOPs.} \quad (10)$$

and the total FLOPs is:

$$\mathcal{C}_{Total} = n_{layers} \cdot 2(4Ld^2 + 2dL^2 + 3Ldm) \approx 8.38 \text{ TFLOPs,} \quad (11)$$

where $L = n + t$, $t = t_s + t_t$ and we use $n=576$, $d=4096$, $m=11008$, $s=35$, $t=20$, and $n_{layers}=32$.

Cost of visual updating in LLaVA-1.5. In LLaVA-1.5, the LLM’s update to visual tokens consists of two main parts: self-attention and FFN. The FLOPs for this visual update are expressed as:

$$\mathcal{C}_{Vis, update} = n_{layers} \times 2 \times (2nd^2 + 2dn^2 + 3ndm). \quad (12)$$

The ratio of the visual update computation to the total visual path computation is given by:

$$\text{Ratio} = \frac{2nd^2 + 2dn^2 + 3ndm}{4nd^2 + 2d(n^2 + nt) + 3ndm}. \quad (13)$$

The visual update computation accounts for more than 80% of the total visual computation. Detailed numerical results are shown in the table 12:

Table 12. Ratio of visual update computation to total visual path computation in LLaVA-1.5.

Model	Visual Update TFLOPs	Total Visual TFLOPs	Ratio (%)
LLaVA-1.5-3B	0.49	3.04	84.0%
LLaVA-1.5-7B	1.24	7.65	83.8%
LLaVA-1.5-13B	2.43	14.91	83.7%

Computation of Our Method. After removing redundant visual pathways, only a small number of text–vision cross-attention layers are retained. In these layers, the remaining vision-related computation consists solely of: (i) the *key–value projection* of vision tokens in attention blocks, and (ii) the *text–vision cross-attention* multiplication in attention block. Their computational costs become:

$$\mathcal{C}_{\text{Vis-Projector}} = n_{\text{retained}} \cdot 2 \cdot 2nd^2, \mathcal{C}_{\text{text-to-vision}} = n_{\text{retained}} \cdot 2 \cdot 2dnt_t. \quad (14)$$

where n_{retained} denotes the number of text–vision cross-attention layers that are retained. Using representative LLaVA-1.5-7B parameters ($n = 576, d = 4096, t_t = 20$), the ratio of these two remaining components is:

$$\frac{\mathcal{C}_{\text{Vis-Projector}}}{\mathcal{C}_{\text{text-to-vision}}} = \frac{2nd^2}{2dnt_t} \approx 204. \quad (15)$$

With the above two components being the only remaining vision-related operations, the overall visual FLOPs after applying our method become:

$$\mathcal{C}_{\text{Vis-Ours}} = n_{\text{retained}} (2nd^2 + 2dnt_t) \approx 0.31 \text{ TFLOPs}. \quad (16)$$

and the corresponding total FLOPs is:

$$\mathcal{C}_{\text{Total-Ours}} = \mathcal{C}_{\text{Vis-Ours}} + n_{\text{layers}} \cdot 2(4td^2 + 2dt^2 + 3tdm) \approx 1.02 \text{ TFLOPs}. \quad (17)$$

where $t = s + t, m = 11008, s = 35, n_{\text{retained}} = 8$, and $n_{\text{layers}} = 32$. At this point, the dominant part of the total computation is contributed by text inference rather than any vision-related operations in the our pruned model.

C.4. Flash attention acceleration implementation

All previous experiments are conducted under the *eager* attention mode, where redundant visual token update paths are removed via explicit masking. As shown in Fig. 8(b), in layers that preserve visual information, visual tokens participate only as key–value pairs in cross-attention, while queries are generated exclusively from text tokens. As a result, the query length is significantly shorter than the key–value length.

FlashAttention naturally supports such asymmetric attention patterns. As illustrated in Fig. 8(a), since FlashAttention v2.1, when $\text{seqlen}_q \neq \text{seqlen}_k$ and $\text{causal}=\text{True}$, the causal mask is aligned to the bottom-right corner of the attention matrix, enabling efficient computation for short-query and long-key–value scenarios. The attention weights produced by our method under FlashAttention are shown in Fig. 8(c). Compared to eager attention, system-prompt tokens exhibit slightly increased attention to visual tokens. However, across multiple benchmarks, this difference results in only minor accuracy degradation in practice. When CUDA utilization is saturated, our approach achieves approximately a $3.5\times$ speedup in the prefill stage, demonstrating the practical efficiency of the proposed architecture under FlashAttention.

D. Details of Comparison Methods

PyramidDrop (Xing et al., 2024a). PyramidDrop is an token pruning method that progressively removes less important tokens across transformer layers to reduce computation while preserving performance. In this work, we apply PDrop to LLaVA-1.5 by discarding half of the remaining tokens at the 1/4, 2/4, and 3/4 depths of the model, without introducing additional learnable parameters. This progressive dropping scheme is equivalent to using approximately 270 tokens per layer on average across the entire network.

YOPO (Zhang et al., 2024). YOPO applies operation-level pruning by reducing visual attention heads, restricting the local visual attention radius, dropping the last vision-related layers, and retaining a fixed ratio of FFN neurons. The detailed pruning settings for each LLaVA-1.5 backbone are summarized in Table 13.

Figure 8. (a) Standard FlashAttention causal masking when the query length differs from the key–value length, where the causal mask is aligned to the bottom-right corner of the attention matrix. (b) Our method under eager attention, where visual tokens are frozen via explicit masking and participate in attention only as key–value representations. (c) Our method under FlashAttention, where visual tokens participate only as key–value and the causal mask is automatically aligned to the bottom-right corner of the attention matrix.

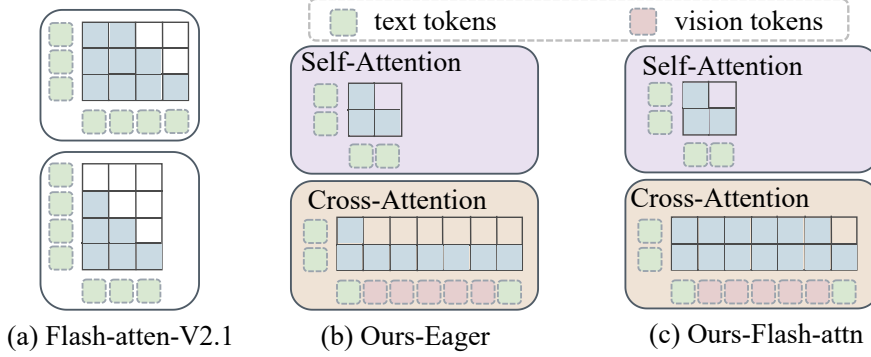


Table 13. YOPO pruning configurations for LLaVA-1.5 models, including the number of retained attention heads (#Heads), local visual attention radius (#Radius), dropped vision layers (#Layers), and retained FFN neuron ratio (#Neurons).

Model	Vision TFLOPs	# Heads	#Radius	# Layers	# Neurons
LLaVA-1.5-3B	0.36	16	5	16	25%
LLaVA-1.5-7B	0.92	16	5	16	25%
LLaVA-1.5-13B	1.79	20	5	20	25%

ToMe (Bolya et al., 2023). ToMe merges similar visual tokens inside Vision Transformers via lightweight token matching, achieving inference acceleration without additional training by reducing redundant token representations.

FastV (Chen et al., 2024b). FastV is the first work to identify redundant visual attention in MLLMs. It performs training-free early-stage token pruning by removing visual tokens with the lowest visual–text attention scores after shallow layers.

SparseVLM (Zhang et al., 2025e). SparseVLM observes that instruction tokens contribute unequally to visual token pruning. It selects instruction tokens most relevant to the visual input and uses their cross-modal attention to guide adaptive, progressive token pruning.

HiRED (Arif et al., 2025). HiRED allocates token budgets across spatial image partitions based on CLS attention. Within each partition, the most informative visual tokens are retained, enabling spatially aware token reduction for high-resolution inputs.

HiPrune (Liu et al., 2025b). HiPrune leverages hierarchical attention patterns in visual encoders and categorizes tokens into anchor, buffer, and register types. It performs training-free pruning while preserving object-centric and global contextual information.

FlowCut (Tong et al., 2025). FlowCut formulates token pruning as an information flow preservation problem, aiming to remove tokens with minimal contribution to the overall information propagation in vision-language models.

HoloV (Zou et al., 2025). HoloV addresses semantic collapse under aggressive pruning by holistically allocating token budgets across spatial regions, ensuring global context coverage and reducing redundancy.

VISA (Jiang et al., 2025). VISA introduces group-wise visual token selection and aggregation via graph summarization. Instead of simply discarding tokens, VISA aggregates information from removed tokens into retained tokens, achieving a favorable efficiency–performance trade-off.

D²Pruner (Zhang et al., 2025b). D²Pruner combines debiased importance estimation with structural diversity. By constructing a hybrid token graph and applying Maximal Independent Set selection, it jointly preserves semantic importance and spatial diversity.

VScan (Zhang et al., 2025a). VScan dynamically scans and selects visual tokens according to task relevance, adapting token retention patterns across different inference stages.

FiCoCo (Han et al., 2024). FiCoCo proposes a unified training-free paradigm termed *Filter–Correlate–Compress* for multimodal token reduction, systematically removing redundancy while preserving key cross-modal correlations.

VisPruner (Zhang et al., 2025c). VisPruner performs visual-only token pruning by combining visual attention-based importance selection with similarity-based duplicate removal, emphasizing visual diversity preservation.

DivPrune (Alvar et al., 2025). DivPrune formulates token pruning as a Max-Min Diversity Problem, selecting a subset of visual tokens by maximizing the minimum pairwise distance among retained tokens.

DOP (Liu et al., 2025a). Depth-wise Operation Pruning (DOP) reduces computation by pruning token-processing operations rather than tokens alone, reallocating saved computation to more informative token groups.

CDPruner (Zhang et al., 2025d). CDPruner introduces conditional diversity maximization for token pruning. It defines visual token similarity conditioned on the instruction context and formulates token selection as a Determinantal Point Process optimization.

Dynamic-LLaVA (Huang et al., 2024). Dynamic-LLaVA applies dynamic sparsification strategies across both prefill and decoding stages, adapting token retention based on KV-cache usage to reduce decoding-time overhead.

TwigVLM (Shao et al., 2025). TwigVLM integrates token pruning with efficient decoding. It combines twig-guided token pruning with self-speculative decoding to improve both inference efficiency and generation speed.

VisionZip (Yang et al., 2025a). VisionZip exploits the high concentration of visual attention in vision encoders. It selects dominant tokens and clusters remaining ones to form contextual tokens, preserving visual information under aggressive compression.

DART (Wen et al., 2025b). DART emphasizes token diversity over individual importance. It iteratively selects visual tokens that are maximally dissimilar to previously selected tokens, reducing redundancy and improving coverage.

TokenPacker (Li et al., 2025b). TokenPacker compresses visual representations at the projector stage using a coarse-to-fine token formation strategy, enabling compact yet informative visual token representations.

Delta-LLaVA (Zamini & Shukla, 2025). Delta-LLaVA introduces low-rank delta projections to compress visual tokens into a compact subspace, maintaining strong performance under fixed small token budgets.

LLaVA-PruMerge (Shang et al., 2025). LLaVA-PruMerge combines pruning and token merging by first removing low-importance tokens using visual attention and then clustering retained tokens based on similarity.

TRIM (Song et al., 2025). TRIM leverages CLIP-based image–text similarity to assess visual token importance, pruning tokens that are weakly aligned with user instructions to improve instruction-aware efficiency.

E. Detail of Benchmark

MME^P (Fu et al., 2023). MME is a widely used benchmark for evaluating multimodal large language models, covering both perceptual and cognitive aspects. In this paper, we consider the perception subset (MME^P), which concentrates on visual understanding through a collection of perception-related tasks (commonly grouped into 14 categories). These tasks

include coarse-grained perception such as object existence, counting, spatial position, and color recognition, as well as fine-grained recognition of posters, celebrities, scenes, landmarks, and artworks, together with OCR-related perception. According to the official evaluation protocol, all questions are posed in a binary (yes/no) format, offering a consistent and controlled assessment of visual perceptual capability.

MMB (Liu et al., 2025c). MMBench is a hierarchical benchmark developed to evaluate multimodal vision–language models across a broad spectrum of perception and reasoning abilities. Its design organizes capabilities into multiple levels of granularity, allowing performance to be analyzed from coarse competencies to more detailed sub-skills. The benchmark adopts a multiple-choice formulation and applies circular evaluation to mitigate scoring variance, supporting reliable and fair model comparison across diverse multimodal scenarios.

MMB^{CN} (Liu et al., 2025c). MMBench-CN serves as the Chinese-language extension of MMBench, aiming to evaluate multimodal understanding under Chinese linguistic settings. It retains the same hierarchical ability structure as the original benchmark while placing emphasis on Chinese-language vision–language alignment. When considered alongside benchmarks in other languages, MMBench-CN also provides insights into multilingual robustness and cross-lingual generalization.

GQA (Hudson & Manning, 2019). GQA is a visual question answering benchmark intended to test structured visual understanding and compositional reasoning. It is built on images from Visual Genome and leverages detailed scene graph annotations that explicitly encode objects, attributes, and relationships. Questions are generated by following well-defined semantic paths over these scene graphs, making GQA particularly suitable for evaluating reasoning grounded in complex visual structures.

VQA^{v2} (Goyal et al., 2017). VQA-v2 is a large-scale, open-ended visual question answering benchmark that examines how models combine visual perception with language understanding and commonsense knowledge. The dataset consists of real-world images paired with open-ended questions, each annotated with multiple human-provided answers. Its adversarially balanced question design reduces language bias, encouraging models to rely more heavily on visual evidence.

SQA^I (Lu et al., 2022). ScienceQA is a multimodal question answering benchmark covering topics from natural sciences, language sciences, and social sciences, with questions organized by topics, categories, and skills. In this work, we evaluate the image-based subset (SQA^I), which includes only questions accompanied by visual inputs. This subset emphasizes multimodal comprehension and scientific reasoning, requiring models to integrate visual information with relevant domain knowledge.

TextVQA (Singh et al., 2019). TextVQA evaluates a model’s ability to recognize and reason about text appearing within natural images. The images contain diverse textual elements, including signs, storefronts, billboards, and product packaging. Successfully answering the questions often involves combining OCR outputs with visual context and semantic reasoning, making TextVQA a representative benchmark for text-centric multimodal understanding.

POPE (Li et al., 2023b). POPE is a diagnostic benchmark designed to analyze object hallucination in vision–language models. It frames hallucination detection as a set of binary questions that ask whether specific objects are present or absent in a given image. By employing multiple sampling strategies and reporting metrics such as accuracy, precision, recall, and F1 score, POPE provides a fine-grained measure of a model’s tendency to hallucinate nonexistent objects.

SEED^I (Li et al., 2024a). SEEDBench is a multiple-choice benchmark for evaluating multimodal understanding. In this study, we focus on the image-only subset (SEED^I), which targets spatial visual understanding and reasoning. The evaluation covers a range of aspects, including scene understanding, object attributes, spatial location, counting, spatial relations, interactions, visual reasoning, and text recognition, offering a structured assessment of image-based vision–language performance.